JACS
JOURNAL OF THE AMERICAN CHEMICAL SOCIETY

Article

Reaction of Ta(NMe) with O: Formation of Aminoxy and Unusual (Aminomethyl)amide Oxo Complexes and Theoretical Studies of the Mechanistic Pathways

Shu-Jian Chen, Xin-Hao Zhang, Xianghua Yu, He Qiu, Glenn P. A. Yap, Ilia A. Guzei, Zhenyang Lin, Yun-Dong Wu, and Zi-Ling Xue

J. Am. Chem. Soc., **2007**, 129 (46), 14408-14421• DOI: 10.1021/ja075076a • Publication Date (Web): 30 October 2007

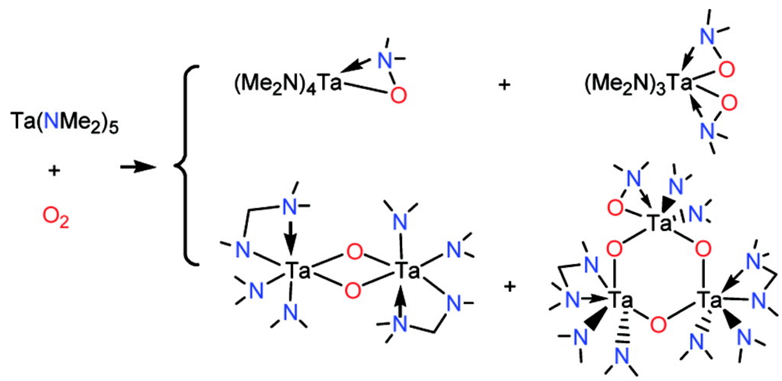

More About This Article

Additional resources and features associated with this article are available within the HTML version:

- Supporting Information
- Links to the 3 articles that cite this article, as of the time of this article download
- Access to high resolution figures
- Links to articles and content related to this article
- Copyright permission to reproduce figures and/or text from this article

View the Full Text HTML

ACS Publications
High quality. High impact.

Journal of the American Chemical Society is published by the American Chemical Society. 1155 Sixteenth Street N.W., Washington, DC 20036

J|A|C|S
ARTICLES
Published on Web 10/30/2007

Reaction of $Ta(NMe_2)_5$ with O_2: Formation of Aminoxy and Unusual (Aminomethyl)amide Oxo Complexes and Theoretical Studies of the Mechanistic Pathways

Shu-Jian Chen,† Xin-Hao Zhang,‡ Xianghua Yu,† He Qiu,† Glenn P. A. Yap,§ Ilia A. Guzei,|| Zhenyang Lin,*,‡ Yun-Dong Wu,*,‡ and Zi-Ling Xue*,†

Contribution from the Department of Chemistry, University of Tennessee, Knoxville, Tennessee 37996, Department of Chemistry, Hong Kong University of Science and Technology, Hong Kong, China, Department of Chemistry and Biochemistry, University of Delaware, Newark, Delaware 19716, and Department of Chemistry, University of Wisconsin, Madison, Wisconsin 53706

Received July 9, 2007; E-mail: chzlin@ust.hk; chydwu@ust.hk; xue@utk.edu

Abstract: Reaction of d^0 $Ta(NMe_2)_5$ (**1**) with O_2 yields two aminoxy complexes $(Me_2N)_nTa(\eta^2\text{-}ONMe_2)_{5-n}$ ($n = 4$, **2**; 3, **3**) as well as $(Me_2N)_4Ta_2[\eta^2\text{-}N(Me)CH_2NMe_2]_2(\mu\text{-}O)_2$ (**4**) and $(Me_2N)_6Ta_3[\eta^2\text{-}N(Me)CH_2NMe_2]_2(\eta^2\text{-}ONMe_2)(\mu\text{-}O)_3$ (**5**) containing novel chelating (aminomethyl)amide $-N(Me)CH_2NMe_2$ ligands. The crystal structures of **2**−**5** have been determined by X-ray crystallography. $(Me_2N)_4Ta(\eta^2\text{-}ONMe_2)$ (**2**) converts to $(Me_2N)_3Ta(\eta^2\text{-}ONMe_2)_2$ (**3**) in its reaction with O_2. In addition, the reaction of $Ta(NMe_2)_5$ with **3** gives **2** only at elevated temperatures. Density functional theory (DFT) calculations have been used to investigate the mechanistic pathways in the reactions of $Ta(NMe_2)_5$ (**1**) with triplet O_2. Monomeric reaction pathways in the formation of **2**−**5** are proposed. A key step is the oxygen insertion into a Ta−N bond in **1** through an intersystem conversion from triplet to singlet energy surface to give an active peroxide complex $(Me_2N)_4Ta(\eta^2\text{-}O\text{-}O\text{-}NMe_2)$ (**A4**). The DFT studies indicate that the peroxide ligand plays an important role, including oxidizing an amide to an imine ligand through the abstraction of a hydride. Insertion of $Me{-}N{=}CH_2$ into a Ta−amide bond yields the unusual $-N(Me)CH_2NMe_2$ ligands.

Reactions of O_2 with metal complexes are important to our understanding of fundamental biological processes and design of oxidation catalysts.[1,2] Most studies of these reactions involve d^n complexes, and oxidation of the metals by O_2 is often a key step. There are, however, fewer studies of reactions of d^0 complexes with O_2.[3,4] In the reactions of O_2 with d^0 alkyl and silyl complexes, O insertion into M−R[3] and M−Si[4a] bonds has been reported. Preparation of d^0 $Mo(NMe_2)_6$, $W(NMe_2)_6$, and WMe_6 requires adventitious O_2.[5] Reactions of d^0 complexes with O_2 have recently been used to yield metal oxides as microelectronic gate-insulating materials.[6−8] With the rapid reduction of the thickness of the gate-insulating layer to less than 2 nm in integrated transistors, SiO_2 with a dielectric constant (κ) of 3.9 is not adequate, leading to a large leakage current.[6] Metal oxides such as Ta_2O_5 ($\kappa = 26$) with large dielectric constants have been actively studied to replace SiO_2 in new generations of microelectronic devices.[6−8] Reactions of O_2 with, e.g., d^0 $Ta(NR_2)_5$ have been used to yield Ta_2O_5 films as gate-insulating materials.[8]

We recently observed that reactions of d^0 $(Me_2N)_4Ta{-}SiR_3$ and $M(NMe_2)_4$ (M = Zr, Hf) with O_2 yielded $(Me_2N)_3Ta(\eta^2\text{-}ONMe_2)(OSiR_3)$[9] and $M_3(NMe_2)_6(\mu\text{-}NMe_2)_3(\mu_3\text{-}O)(\mu_3\text{-}ONMe_2)$,[10] respectively. The nature of the reactions between d^0 amides and

† University of Tennessee.
‡ Hong Kong University of Science and Technology.
§ University of Delaware.
|| University of Wisconsin.

(1) See, e.g.: (a) Kopp, D. A.; Lippard, S. J. *Curr. Opin. Chem. Biol*. **2002**, *6*, 568. (b) Theopold, K. H.; Reinaud, O. M.; Blanchard, S.; Leelasubcharoen, S.; Hess, A.; Thyagarajan, S. *ACS Symp. Ser*. **2002**, *823*, 75. (c) Que, L.; Jr.; Tolman, W. B. *Angew. Chem., Int. Ed.* **2002**, *41*, 1114. (d) Stahl, S. S. *Science* **2005**, *309*, 1824. (e) Keith, J. M.; Muller, R. P.; Kemp, R. A.; Goldberg, K. I.; Goddard, W. A., III; Oxgaard, J. *Inorg. Chem.* **2006**, *45*, 9631. (f) Popp, B. V.; Stahl, S. S. *J. Am. Chem. Soc.* **2007**, *129*, 4410 and references therein.
(2) Simándi, L. I., Ed. *Advances in Catalytic Activation of Dioxygen by Metal Complexes*; Kluwer: Boston, 2003.
(3) (a) Labinger, J. A.; Hart, D. W.; Seibert, W. E.; Schwartz, J. *J. Am. Chem. Soc.* **1975**, *97*, 3851. (b) Lubben, T. V.; Wolczanski, P. T. *J. Am. Chem. Soc.* **1987**, *109*, 424. (c) Brindley, P. B.; Scotton, M. J. *J. Chem. Soc., Perkin Trans.* **1981**, 419. (d) Wang, R.; Folting, K.; Huffman, J. C.; Chamberlain, L. R.; Rothwell, I. P. *Inorg. Chem. Acta* **1986**, *120*, 81. (e) Gibson, V. C.; Redshaw, C.; Walker, G. L. P.; Howard, J. A. K.; Hoy, V. J.; Cole, J. M.; Kuzmina, L. G.; De Silva, D. S. *J. Chem. Soc., Dalton Trans.* **1999**, 161. (f) Van Asselt, A.; Trimmer, M. S.; Healing, L. M.; Bercaw, J. E. *J. Am. Chem. Soc.* **1988**, *110*, 8254. (g) Brindley, P. B.; Hodgson, J. C. *J. Organomet. Chem.* **1974**, *65*, 57. (h) Gibson, T. *Organometallics* **1987**, *6*, 918. (i) Kim, S.-J.; Jung, I. N.; Yoo, B. R.; Cho, S.; Ko, J.; Kim, S. H.; Kang, S. O. *Organometallics* **2001**, *20*, 1501.
(4) (a) Tilley, T. D. *Organometallics* **1985**, *4*, 1452. (b) A bisperoxo complex was observed in the reaction of a Zr(IV) amide complex with O_2. Stanciu, C.; Jones, M. E.; Fanwick, P. E.; Abu-Omar, M. M. *J. Am. Chem. Soc.* **2007**, *129*, 12400.
(5) (a) Bradley, D. C.; Chisholm, M. H.; Extine, M. W. *Inorg. Chem.* **1977**, *16*, 1791. (b) Chisholm, M. H.; Hammond, C. E.; Huffman, J. C. *J. Chem. Soc., Chem. Commun*. **1987**, 1423. (c) Galyor, L.; Mertis, K.; Wilkinson, G. *J. Organomet. Chem.* **1975**, *85*, C37.
(6) (a) Wallace, R. M.; Wilk, G. D. *Crit. Rev. Solid State Mater. Sci.* **2003**, *28*, 231. (b) Smith, R. C.; Ma, T.; Hoilien, N.; Tsung, L. Y.; Bevan, M. J.; Colombo, L.; Roberts, J.; Campbell, S. A.; Gladfelter, W. L. *Adv. Mater. Opt. Electron.* **2000**, *10*, 105.
(7) (a) Bastianini, A.; Battiston, G. A.; Gerbasi, R.; Porchia, M.; Daolio, S. *J. Phys. IV* **1995**, *5*(C5), 525. (b) Ohshita, Y.; Ogura, A.; Hoshino, A.; Hiiro, S.; Machida, H. *J. Cryst. Growth* **2001**, *233*, 292.
(8) Son, K.-A.; Mao, A. Y.; Sun, Y.-M.; Kim, B. Y.; Liu, F.; Kamath, A.; White, J. M.; Kwong, D. L.; Roberts, D. A.; Vrtis, R. N. *Appl. Phys. Lett.* **1998**, *72*, 1187.
(9) Wu, Z.-Z.; Cai, H.; Yu, X.-H.; Blanton, J. R.; Diminnie, J. B.; Pan, H.-J.; Xue, Z.-L. *Organometallics* **2002**, *21*, 3973.
(10) Wang, R.; Zhang, X.-H.; Chen, S.-J.; Yu, X.; Wang, C.-S.; Beach, D. B.; Wu, Y.-D.; Xue, Z.-L. *J. Am. Chem. Soc.* **2005**, *127*, 5204.

10.1021/ja075076a CCC: $37.00

Scheme 1. Formation of **2**−**5** from the Reaction of Ta(NMe$_2$)$_5$ (**1**) with O$_2$

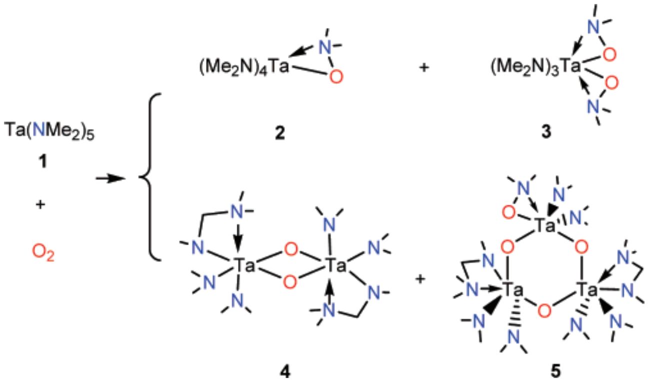

O$_2$ is still largely unknown.[6−8] We have found that the reaction of Ta(NMe$_2$)$_5$ (**1**) with O$_2$ gives unusual oxo complexes (Me$_2$N)$_4$Ta$_2$[η^2-N(Me)CH$_2$NMe$_2$]$_2$(μ-O)$_2$ (**4**) and (Me$_2$N)$_6$Ta$_3$-[η^2-N(Me)CH$_2$NMe$_2$]$_2$(η^2-ONMe$_2$)(μ-O)$_3$ (**5**) containing novel chelating −N(Me)CH$_2$NMe$_2$ ligands[11] as well as aminoxy complexes (Me$_2$N)$_4$Ta(η^2-ONMe$_2$) (**2**) and (Me$_2$N)$_3$Ta(η^2-ONMe$_2$)$_2$ (**3**) (Scheme 1). This reaction is a rare case of the formation of oxo ligands (in **4** and **5**) in the reactions of d^0 complexes with O$_2$.[10,12] Density functional theory (DFT) studies suggest monomeric reaction pathways in the formation of **2**−**5** through peroxide intermediates. The abstraction of a hydride from a −NMe$_2$ ligand by a peroxide ligand leads to the formation of imine MeN═CH$_2$, which then inserts into a Ta−NMe$_2$ bond to give the novel η^2-N(Me)CH$_2$NMe$_2$ ligands. Our experimental and theoretical studies are reported.

Results and Discussion

Formation and Characterization of 2−5. Reaction of O$_2$ (0.5 equiv, 650 mmHg) with Ta(NMe$_2$)$_5$ (**1**) in toluene gave **2**, **3**, and **4** in 46−52%, 8−9%,[13] and 8−9% yields (based on O$_2$), respectively, by ^{1}H NMR. Crystallization of the mixture, discussed below, gave **2**, **3**, and **4** in 27%, 12%,[13] and 7% isolated yields. When 1.0 equiv of O$_2$ (570 mmHg) was used in an NMR tube, the yield of **2** dropped to 26−27%, while that of **3** increased to 34−37%. The yield of **4** at 9−10% was similar to 8−9% from 0.5 equiv of O$_2$.

Initial crystallization of the reaction mixture at −32 °C yielded colorless crystals of dimeric **4**. A few crystals of **5** were sometimes found along with those of **4**, and X-ray crystallography confirmed the identity of the crystals of **5** isolated from the mixture. ^{1}H NMR spectrum of the mixture of the crystals in benzene-d_6, however, failed to reveal the presence of **5**, suggesting that the yield of **5** in the reaction is perhaps below the detection limit of ^{1}H NMR. **5** was prepared separately from the reaction of excess O$_2$ (4 equiv) with Ta(NMe$_2$)$_5$ (**1**) and characterized by NMR spectroscopy, which is discussed below.

After the crystallization to isolate **4**, removing volatiles from the supernatant solution gave a yellow, oily mixture, which upon sublimation at 55 °C yielded a pale-yellow solid of **2**. Crystallization of the solid gave colorless crystals of **2**. Dissolving the pale-yellow residue of the sublimation in *n*-pentane and subsequent crystallization yielded colorless crystals of **3**.

The molecular structures of **2**−**5** are shown in Figure 1. Crystallographic data for **2**−**5** are given in Table 1.[14] Selected bond lengths and angles are listed in Table 2.

(Me$_2$N)$_4$Ta(η^2-ONMe$_2$) (**2**) was also prepared from the reaction of (Me$_2$N)$_4$TaCl with 1 equiv of LiONMe$_2$ (eq 1). Its reactivity toward O$_2$ is discussed below. In the molecular structure of **2**, one O inserted into a Ta−N bond to form a monomer, yielded an O−Ta covalent bond and a N−Ta dative bond in a distorted octahedral geometry with a nearly linear N(3)−Ta−N(4) angle of 172.9(4)°. Only one peak in the ^{1}H (3.25 ppm) or the ^{13}C (48.80 ppm) NMR spectrum of **2** is observed for the four −NMe$_2$ ligands, suggesting that **2** undergoes a fast ligand-site exchange.

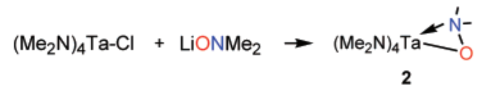 (1)

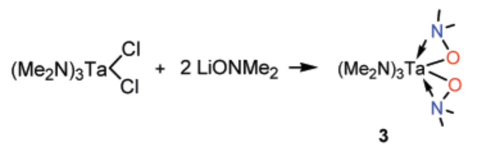 (2)

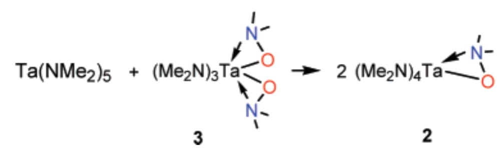 (3)

(Me$_2$N)$_3$Ta(η^2-ONMe$_2$)$_2$ (**3**) is thermally stable. It was also prepared from the reaction of (Me$_2$N)$_3$TaCl$_2$ with 2 equiv of LiONMe$_2$ (eq 2). **3** shows a distorted pentagonal bipyramidal geometry with two axial −NMe$_2$ ligands and a nearly linear N(1)−Ta−N(3) angle of 178.2(2)°. The equatorial −NMe$_2$ and two η^2-ONMe$_2$ ligands are coplanar[15] with two dative Ta←N bonds. The two O atoms face each other. The ^{1}H and ^{13}C NMR spectra of **3** at 23 °C show three peaks (^{1}H NMR: 3.41, 3.05, and 2.94 ppm in a 1:1:1 ratio; ^{13}C NMR: 48.98, 47.05, 46.11 ppm) for the equatorial and two axial −N*Me*$_2$ ligands. This observation suggests that (1) the two axial −NMe$_2$ ligands do not undergo a fast rotation at 23 °C, probably as a result of M−N d−p π bonding in this otherwise electron-deficient complex; (2) there is no axial−equatorial exchange among the three −NMe$_2$ ligands on the NMR time scale at 23 °C. Thus, the two methyl groups in each axial amide are not equivalent (−NMe_AMe_B). They are close to the equatorial −NMe$_2$ and O atoms, respectively. EXSY NMR studies revealed exchanges among the amide ligands.[14] Variable-temperature (VT) NMR studies showed coalescences among the three −NMe$_2$ ligands in **3** at high temperatures. The EXSY and VT NMR spectra are given in the Supporting Information. At 60 °C, the peaks at 2.94 and 3.05 ppm merge into one broad peak at 3.00 ppm with a rate constant of 100 s^{-1} ($\Delta G_{333K}^{\ddagger}$ = 17 kcal/mol), suggesting that these two peaks are those of Me_a and Me_b groups in the axial amide ligands. At 70 °C this new peak further coalesced with that of the equatorial −NMe$_2$ with a rate constant of 163 s^{-1} ($\Delta G_{343K}^{\ddagger}$ = 17 kcal/mol) for the axial → equatorial exchange.[14] An alternative explanation is that there is only one

(11) Our searches of the SciFinder and Beilstein data bases for −N(Me)CH$_2$-NR$_2$ (R = Me, Et, Pr^i) ligands and their parent amines yielded only the following Japanese patent about HN(Me)CH$_2$NEt$_2$: Aron-Samuel, J. M. D. *Jpn. Tokkyo Koho*, JP 53017595 19780609, 1978. MeNHCH$_2$NMe$_2$ was the subject of calculations in Carballeira, L.; Perez-Juste, I. *J. Comput. Chem.* **2001**, *22*, 135.
(12) Chen, T.-N.; Wu, Z.-Z.; Li, L.-T.; Sorasaenee, K. R.; Diminnie, J. B.; Pan, H.-J.; Guzei, I. A.; Rheingold, A. L.; Xue, Z.-L. *J. Am. Chem. Soc*. **1998**, *120*, 13519.
(13) The difference between the 8−9% yield of **3** estimated by ^{1}H NMR and its 12% isolated yield is probably due to the error in NMR integration.
(14) See Supporting Information for details.
(15) Distances of N2, N4, and O1 to the Ta−O2−N5 plane are 0.0460, 0.0352, and 0.0151 Å, respectively.

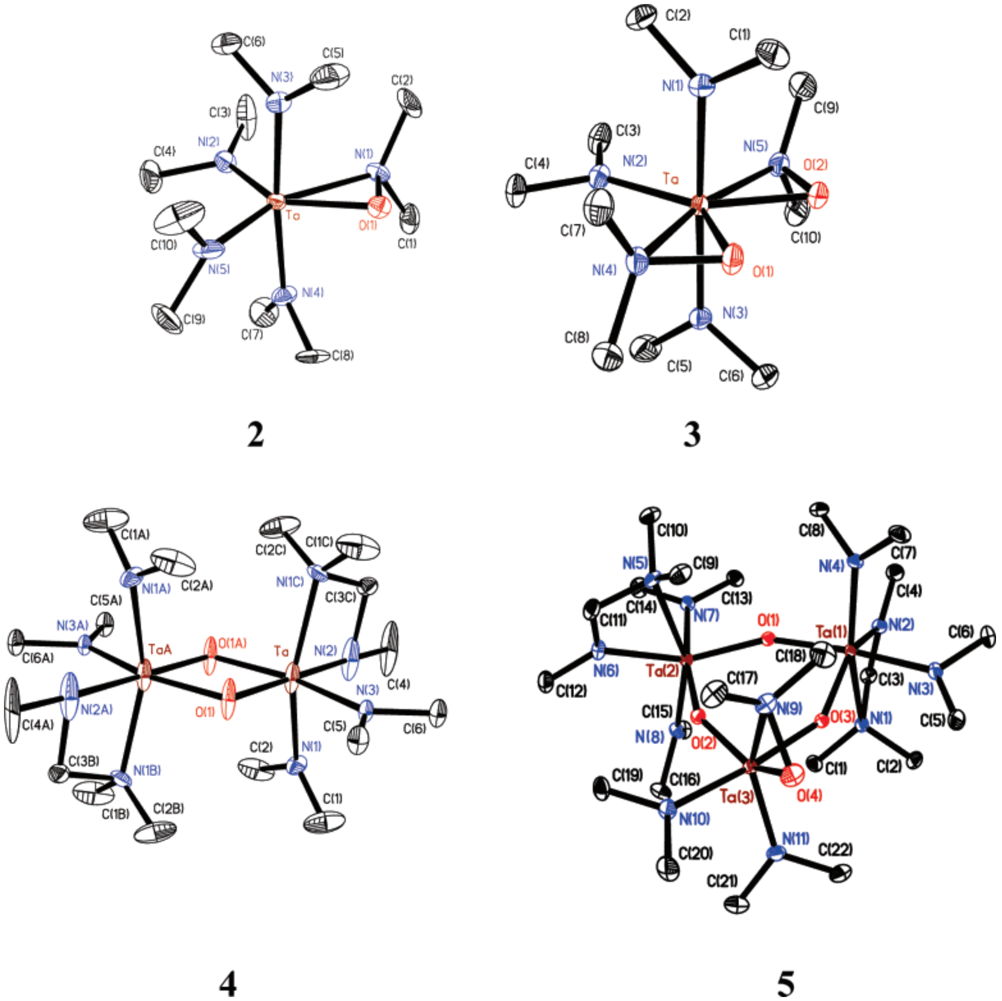

Figure 1. ORTEP views of **2**−**5**. Disorder was observed in **4**.

exchange of the ligands: axial−equatorial exchange of the $-NMe_2$ ligands. As the equatorial $-NMe_2$ ligand moves to the axial position, its two methyl groups move to the Me_a and Me_b positions. The fact that the activation free energies $\Delta G_{333K}^{\ddagger}$ and $\Delta G_{343K}^{\ddagger}$ are equal suggests that the three amide ligands are exchanging via the same process.

$(Me_2N)_4Ta_2[\eta^2\text{-}N(Me)CH_2NMe_2]_2(\mu\text{-}O)_2$ (**4**) exhibits a dimeric, centrosymmetric structure with two oxo bridges between Ta atoms (Figure 1). The Ta−O(1)−TaA angle of 103.6(4)° in the Ta−O(1)−TaA−O(1A) four-member ring is much larger than the O(1)−Ta−O(1A) angle of 76.4(4)°. The Ta−O bond lengths of 1.932(9)−1.958(10) Å are close to 1.917(6)−1.928(6) Å in $[TaCl_2(NMe_2)_2(HNMe_2)]_2O$[16] containing a single O bridge between two Ta atoms.

Crystals of **4** are thermally stable at −32 °C, but **4** in benzene-d_6 under N_2 was found to decompose in one week at 23 °C. In the ^{1}H NMR spectrum of **4**, the peaks of the $-NMe_2$ and the $-NMe$ groups in the chelating $-N(Me)CH_2NMe_2$ ligands are at 2.39 and 3.22 ppm, respectively. The former ($-NMe_2$) is an amine group and donates its lone pair electrons to the Ta atoms. The latter ($-NMe$) is an amide ligand carrying a negative charge, and its chemical shift is close to 3.51 ppm for the terminal $-NMe_2$ ligands in **4**. The methylene protons in the chelating $-N(Me)CH_2NMe_2$ ligands appear as a singlet at 4.19 ppm, downfield shifted from those of the methyl groups in **4**. In the ^{13}C NMR spectrum at 23 °C, the resonance of the methylene carbon at 83.06 ppm is also downfield shifted from those of the methyl groups in **4**. **4** is inert to O_2. Its solution in benzene-d_6 was found to slowly decompose to $HNMe_2$ and unknown Ta species.

As noted earlier, crystals of $(Me_2N)_6Ta_3[\eta^2\text{-}N(Me)CH_2NMe_2]_2(\eta^2\text{-}ONMe_2)(\mu\text{-}O)_3$ (**5**) were sometimes found along with the crystals of **4** in the separation of **4** from the reaction of O_2 (0.5 equiv) with $Ta(NMe_2)_5$ (**1**). The identity of **5** in the crystal mixture was confirmed by single-crystal X-ray diffraction. However, NMR spectra of the crystal mixture showed only the resonances of **4**. When 4 equiv of O_2 was used to react with **1**, a mixture of crystals of **4** and **5** was again obtained. ^{1}H NMR spectra of the mixture gave the resonances of **5**, indicating that the reaction of **1** with 4 equiv of O_2 gave a higher yield (0.52%) of **5**.

5 is a trimetallic complex containing three oxo bridges (Figure 1). Two Ta atoms [Ta(1) and Ta(2)] each and the third Ta atom [Ta(3)] are coordinated by one η^2-$N(Me)CH_2NMe_2$ ligand and a η^2-$ONMe_2$ ligand, respectively. In addition, two $-NMe_2$ ligands on each Ta atom give a pseudo-octahedral environment around the metal. There is no symmetry in the solid structure of **5**, making each ligand unique. The MeN− and $-NMe_2$ moieties of both η^2-$N(Me)CH_2NMe_2$ ligands are *trans* to an

(16) Chisholm, M. H.; Huffman, J. C.; Tan, L.-S. *Inorg. Chem.* **1981**, *20*, 1859.

Table 1. Crystal Data and Structure Refinement for **2**−**5**

	2	**3**	**4**	**5**
emp. formula (fw)	$C_{10}H_{30}N_5OTa$ (417.34)	$C_{10}H_{30}N_5O_2Ta$ (433.34)	$C_{16}H_{46}N_8O_2Ta_2$ (744.51)	$C_{25.5}H_{68}N_{11}O_4Ta_3$ (1135.76)
temp (K)	173(2)	173(2)	120(2)	100(2)
crystal system	orthorhombic	monoclinic	monoclinic	triclinic
space group	*Pca*2(1)	*P*2(1)/*n*	*C*2/*m*	$P\bar{1}$
unit cell dimensions (Å and deg)	$a = 17.079(6)$, $\alpha = 90$, $b = 12.092(4)$, $\beta = 90$, $c = 16.206(5)$, $\gamma = 90$	$a = 8.273(9)$, $\alpha = 90$, $b = 13.077(14)$, $\beta = 99.880(18)$, $c = 16.250(17)$, $\gamma = 90$	$a = 11.435(6)$, $\alpha = 90$, $b = 13.712(8)$, $\beta = 107.534(7)$, $c = 8.616(5)$, $\gamma = 90$	$a = 9.8785(5)$, $\alpha = 77.972(1)$, $b = 11.5811(5)$, $\beta = 82.666(1)$, $c = 19.2869(9)$, $\gamma = 66.618(1)$
volume (Å^3)	3346.9(19)	1732(3)	1288.1(12)	1978.35(16)
Z	8	4	2	2
density (calcd, Mg/m^3)	1.920	1.657	1.662	1.907
ab. coeff. (mm^{-1})	6.565	6.350	8.514	8.318
F(000)	1648	856	720	1098
crystal size (mm^3)	0.38 × 0.32 × 0.27	0.25 × 0.14 × 0.12	0.20 × 0.10 × 0.04	0.38 × 0.34 × 0.31
θ range (deg)	2.06 to 28.32	2.01 to 28.29	2.39 to 28.21	1.95 to 29.50
index ranges	$-21 \leq h \leq 22$, $-15 \leq k \leq 15$, $-20 \leq l \leq 21$	$-10 \leq h \leq 10$, $-17 \leq k \leq 17$, $-21 \leq l \leq 21$	$-15 \leq h \leq 14$, $-17 \leq k \leq 18$, $-11 \leq l \leq 11$	$-13 \leq h \leq 13$, $-16 \leq k \leq 16$, $-26 \leq l \leq 26$
reflections collected	32990	18076	7190	36051
indep. reflections	7935 [*R*(int) = 0.0596]	4170 [*R*(int) = 0.0372]	1565 [*R*(int) = 0.0529]	10805 [*R*(int) = 0.0262]
completeness to θ =	28.32°, 98.1%	28.29°, 97.0%	25.00°, 100.0%	29.50°, 98.1%
max./min. transmission	0.2702/ 0.1893	0.5162/ 0.2997	0.7270/ 0.2808	0.1825/ 0.1442
data/restraints/param.	7935/1/327	4170/0/173	1565/0/79	10805/0/381
goodness-of-fit on F^2	1.163	1.167	1.060	1.045
final *R* indices [$I > 2\sigma(I)$]^a	R1 = 0.0388, wR2 = 0.0945	R1 = 0.0248, wR2 = 0.0620	R1 = 0.0566, wR2 = 0.1576	R1 = 0.0201, wR2 = 0.0493
R indices (all data)	R1 = 0.0536, wR2 = 0.1229	R1 = 0.0360, wR2 = 0.0882	R1 = 0.0576, wR2 = 0.1591	R1 = 0.0238, wR2 = 0.0505
largest diff. peak and hole	3.786 and −2.130 e·Å^{-3}	1.128 and −2.190 e·Å^{-3}	2.691 and −3.269 e·Å^{-3}	2.316 and −0.911 e·Å^{-3}

^{a} $R = \Sigma||F_o| - |F_c||/\Sigma|F_o|$; $R_w = (\Sigma[w(F_o^2 - F_c^2)^2]/\Sigma[w(F_o^2)^2])^{1/2}$.

oxo and amide ligand, respectively. The O(4) atom in the η^2-ONMe$_2$ ligand is nearly trans to bridging O(2) with the O(4)−Ta(3)−O(2) angle of 143.82(8)°. The Ta(3)−O(2) bond length of 1.8845(17) Å is shorter than other Ta−oxo bond lengths [1.9404(17)−1.9988(17) Å] and the Ta(3)−O(4)NMe$_2$ length of 2.028(2) Å. In the six-membered ring formed by the three oxo ligands and three Ta atoms, the Ta−O−Ta angles range from 148.35(10) to 154.89(10)°, significantly larger than that [103.6(4)°] in dimeric **4**. The O−Ta−O angles are nearly 90° [87.07(7)−92.92(8)°], as expected for the octahedral-coordinated Ta atoms. **5** provides an accurate structure of the novel η^2-N(Me)CH$_2$NMe$_2$ ligand, as those in **4** are both disordered. In **5**, the Ta−N(Me) bond lengths of 2.037(2)−2.042(2) Å are similar to those [2.003(2)−2.042(2) Å] in Ta−NMe$_2$ (monodentate); however, they are significantly smaller than those of dative Ta←NMe$_2$ bonds [2.393(2)− 2.394(2) Å] in the η^2-N(Me)CH$_2$NMe$_2$ ligands. Both ^{1}H and ^{13}C NMR spectra of **5** are consistent with its structure, and the chemical shifts of the η^2-N(Me)CH$_2$NMe$_2$ and η^2-ONMe$_2$ ligands in **5** are similar to those in **4** and **2**−**3**, respectively.

Repeated attempts were made to characterize (Me$_2$N)$_3$Ta(η^2-ONMe$_2$)$_2$ (**3**) by mass spectrometry (MS) using electron ionization (EI), DART (direct analysis in real time),[17] and electrospray ionization (ESI). These spectra, however, did not reveal the parent ion or [**3** + H$^+$] peak.[14] Similarly the spectrum of (Me$_2$N)$_4$Ta$_2$[η^2-N(Me)CH$_2$NMe$_2$]$_2$(μ-O)$_2$ (**4**) using EI did not reveal its parent ion peak. Thus, no attempts were made to conduct crossover studies using a Ta(NMe$_2$)$_5$−Ta(NMe$_2$-d_6)$_5$ mixture or investigate whether the two O atoms in either **3** or **4** were from the same O$_2$ molecules using a ^{16}O$_2$−^{18}O$_2$ mixture. Such studies would rely on the characterization of isotopomers by MS.

Reaction of Ta(NMe$_2$)$_5$ (1) with O$_2$ at −50 °C or a Lower Pressure of O$_2$. The reaction was conducted at −50 °C with 0.5 equiv of O$_2$ and monitored by ^{1}H NMR. (Me$_2$N)$_4$Ta(η^2-ONMe$_2$) (**2**) was the first *observed* product by ^{1}H NMR in 23 min. However, this does not necessarily indicate that **2** was the first product in the reaction, as we cannot rule out that other products had formed at concentrations below the NMR detection limit. **3** and **4** were observed later in 40 min.

Effect of O$_2$ pressure on its reaction with **1** was studied as well. The partial pressure of O$_2$ (0. 5 equiv) in sealed reaction flasks varied between 240 (Sample A), 500 (Sample B), and 760 mmHg (Sample C), respectively. In 24 min, **1** in Sample C had all disappeared. After 32 min, 5.5% of unreacted **1** was observed in Sample B. In comparison, after 39 min, 21.8% of unreacted **1** was observed in Sample A. Although these studies are limited in scope, the observations indicate that the reaction at a higher O$_2$ partial pressure is faster.

After 19 h, ^{1}H NMR spectra show that the yields of

(17) Cody, R. B.; Laramee, J. A.; Durst, H. D. *Anal. Chem.* **2005**, *77*, 2297.

Table 2. Selected Bond Lengths and Angles in **2**−**5**

2	**3**	**4**	**5**
O(1)−Ta 1.983(7)	Ta−N(1) 2.052(5)	Ta−O(1) 1.932(9)	Ta(1)−O(3) 1.9404(18)
N(1)−Ta 2.288(10)	Ta−N(2) 2.029(5)	Ta−O(1A) 1.958(10)	Ta(1)−O(1) 1.9723(17)
N(2)−Ta 1.969(10)	Ta−N(3) 2.065(5)	Ta−N(1) 2.234(8)	Ta(2)−O(1) 1.9365(17)
N(3)−Ta 2.064(10)	Ta−N(4) 2.203(5)	Ta−N(2) 1.957(14)	Ta(2)−O(2) 1.9988(17)
N(4)−Ta 2.057(10)	Ta−N(5) 2.234(5)	Ta−N(3) 2.040(11)	Ta(3)−O(2) 1.8845(17)
N(5)−Ta 2.002(11)	Ta−O(1) 2.014(5)	Ta−O(1)−TaA 103.6(4)	Ta(3)−O(3) 1.9554(18)
N(2)−Ta−O(1) 133.2(4)	Ta−O(2) 2.016(5)	N(2)−Ta−O(1A) 104.0(5)	Ta(3)−O(4) 2.028(2)
O(1)−Ta−N(5) 116.6(5)	N(5)−O(2) 1.462(7)	O(1)−Ta−N(1) 103.7(2)	O(4)−N(9) 1.436(3)
O(1)−Ta−N(4) 88.5(4)	N(4)−O(1) 1.448(6)	N(2)−Ta−N(1) 76.3(2)	Ta(1)−N(1) 2.394(2)
O(1)−Ta−N(3) 85.3(4)	N(1)−Ta−N(2) 90.1(2)		Ta(1)−N(2) 2.042(2)
O(1)−Ta−N(1) 38.8(3)	N(1)−Ta−N(4) 90.7(2)		Ta(1)−N(3) 2.042(2)
O(1)−N(1)−Ta 59.1(4)	N(1)−Ta−N(5) 89.9(2)		Ta(1)−N(4) 2.015(2)
	N(1)−Ta−N(3) 178.2(2)		Ta(2)−N(5) 2.393(2)
	O(1)−Ta−N(1) 89.4(2)		Ta(2)−N(6) 2.037(2)
	O(1)−Ta−N(4) 39.85(18)		Ta(2)−N(7) 2.031(2)
	O(1)−Ta−O(2) 87.17(18)		Ta(2)−N(8) 2.003(2)
			O(3)−Ta(1)−O(1) 87.07(7)
			O(1)−Ta(2)−O(2) 84.52(7)
			O(2)−Ta(3)−O(3) 90.35(8)
			O(3)−Ta(3)−O(4) 92.92(8)
			O(2)−Ta(3)−O(4) 143.82(8)
			Ta(2)−O(1)−Ta(1) 154.89(10)
			Ta(3)−O(2)−Ta(2) 151.38(10)
			Ta(1)−O(3)−Ta(3) 148.35(10)
			Ta(2)−O(1)−Ta(1) 154.89(10)
			Ta(3)−O(2)−Ta(2) 151.38(10)
			Ta(1)−O(3)−Ta(3) 148.35(10)
			N(9)−O(4)−Ta(3) 78.12(13)

Scheme 2

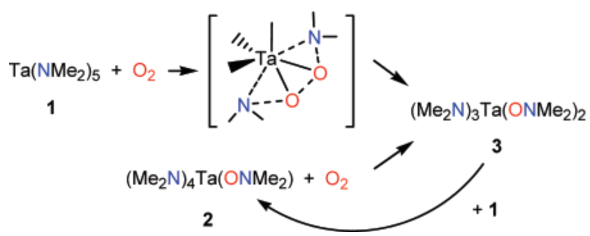

$Ta(NMe_2)_3(\eta^2\text{-}ONMe_2)_2$ (**3**) and $(Me_2N)_4Ta_2[\eta^2\text{-}N(Me)CH_2\text{-}NMe_2]_2(\mu\text{-}O)_2$ (**4**) in the three samples were similar: 5−7% of **3** and 7−11% of **4**. The yields of $Ta(NMe_2)_4(\eta^2\text{-}ONMe_2)$ (**2**) in Samples B and C were similar (49−55%) and higher than 35% in Sample A (that was exposed to 240 mmHg O_2). As discussed earlier, the yield of **5** was too small to be detected by NMR in the reaction mixture. It should be noted that the yields of **2**−**4** in Samples B (500 mmHg) and C (760 mmHg) are similar to those (46−52% **2**, 8−9% **3**, 8−9% **4**) yielded with 650 mmHg (0.5 equiv) O_2 discussed earlier.

Reaction of $(Me_2N)_4Ta(\eta^2\text{-}ONMe_2)$ (2) with O_2 and an Exchange between $Ta(NMe_2)_5$ (1) and $(Me_2N)_3Ta(\eta^2\text{-}ONMe_2)_2$ (3). Additional studies have been conducted to shed light on the formation of **2** and **3**. **2** was found to react with 1 equiv of O_2 to give **3** in 43% yield (based on **2**, Scheme 2), suggesting that **2** is perhaps an intermediate to **3**. However, this observation cannot rule out the formation of **3** from direct insertion of two O atoms of an O_2 molecule into two Ta−N bonds in **1**. Our earlier theoretical studies of the reactions of O_2 with model complexes $Zr(NR_2)_4$ (R = Me, H) in fact suggest that such pathways are feasible.[10] In other words, two parallel pathways in Scheme 2 may both lead to the formation of **3**.

Heating a mixture of $Ta(NMe_2)_5$ (**1**) and $(Me_2N)_3Ta(\eta^2\text{-}ONMe_2)_2$ (**3**) in a sealed Young NMR tube at 50 °C for 4 days yielded no change in the ^{1}H NMR spectrum. After heating the mixture at 90 °C for another 3 days, a significant amount of $(Me_2N)_4Ta(\eta^2\text{-}ONMe_2)$ (**2**) (eq 3) was formed, suggesting that there is a larger barrier for this exchange. Our theoretical studies, discussed below, are consistent with the observation. The DFT calculations suggest that this exchange occurs in the presence of a catalyst to give **2**. On the basis of the results thus far, a partial picture of the pathways in the formation of **2** and **3** is provided in Scheme 2. The cycle in the conversions between **2** and **3** uses both **1** and O_2 until the limiting reagent is consumed.

Reaction of $Ta(NMe_2)_5$ (1) with O_2 in the Presence of a Radical Trap. The products of the reaction between **1** and O_2 may also be derived from an autoxidation path involving radical initiation and propagation. In other words, free radicals are expected to be present during the reaction. We conducted the reaction of $Ta(NMe_2)_5$ (**1**) with O_2 in the presence of TEMPO (1,1,5,5-tetramethylpentamethylene nitroxide) as a radical trap.[14,18] ^{1}H NMR monitoring of the reaction revealed that (1) **1** slowly reacts with TEMPO, giving unknown species;[18] (2) most TEMPO (90%) remained after the reaction between **1** and O_2 was completed; (3) no products of radical trapping by TEMPO could be identified; (4) products identical to those in the absence of TEMPO (**2**−**4**, $HNMe_2$) were observed in the reaction, except for the unidentified species from the slow reaction of **1** with TEMPO. The study here, limited in scope, could not rule out autoxidation as a pathway in the reaction. It suggests, however, that, if autoxidation is a pathway, it is perhaps not the main pathway. Our theoretical studies of the pathways are given below.

DFT Studies of the Reaction between d^0 $Ta(NMe_2)_5$ (1) and O_2. To extend our understanding of the reactions of d^0 transition metal amide complexes with O_2,[10] the mechanistic pathways of the reaction of **1** with O_2 have been investigated by DFT calculations.

(18) Albéniz, A. C.; Espinet, P.; López-Fernández, R.; Sen, A. *J. Am. Chem. Soc.* **2002**, *124*, 11278.

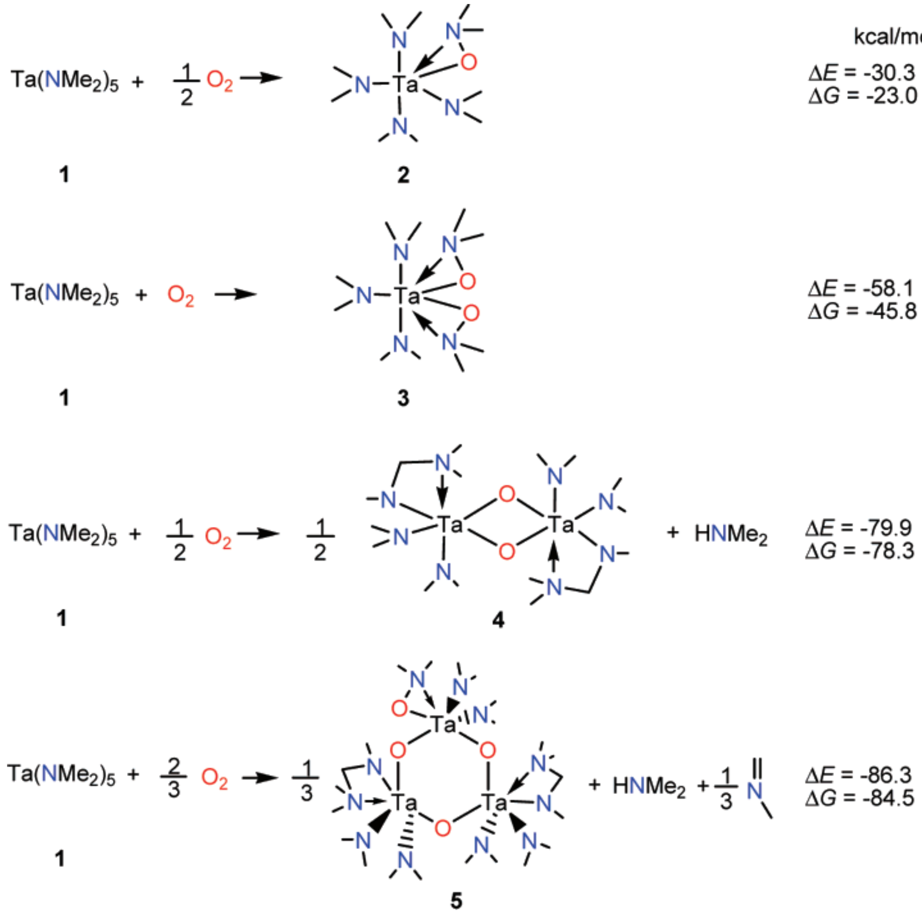

Figure 2. Reaction energies and reaction free energies at 298.15 K calculated for the reactions of **1** with O_2 leading to the formations of **2**−**5**.

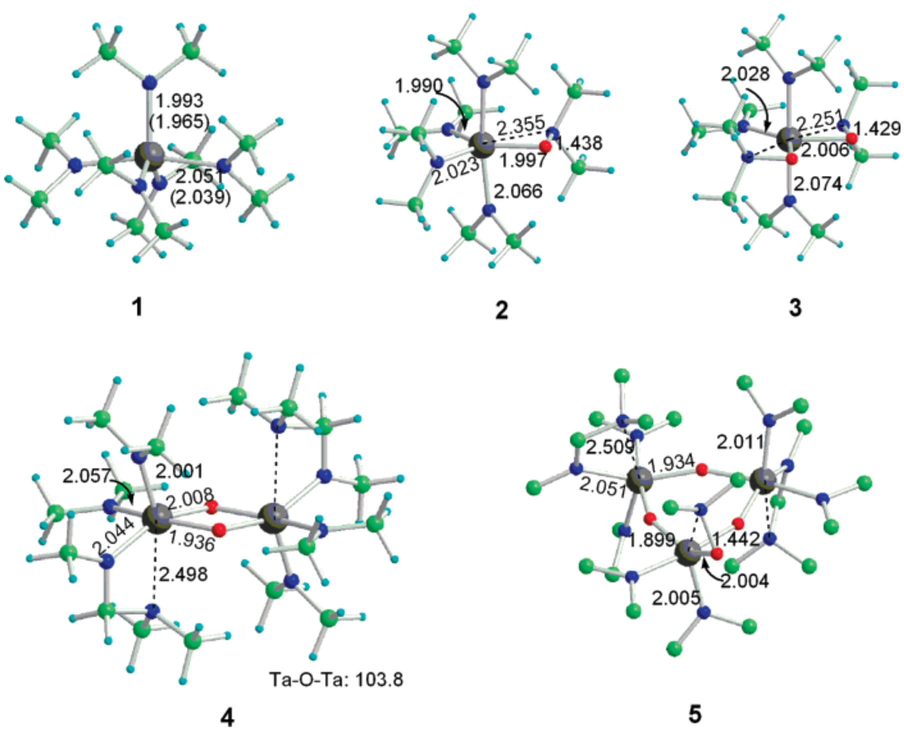

Figure 3. Optimized structures with selected bond lengths (Å) and angles (deg) for **1**−**5**. The corresponding X-ray structural parameters are given in parentheses. The hydrogen atoms in **5** are omitted for clarity.[19]

We first studied the reaction of **1** with O_2 to form the experimentally observed products **2**−**5**. The calculated reaction energies and geometries of **2**−**5** are shown in Figures 2 and 3. The calculated Ta−N(amide) bonds are in good agreement with those of the X-ray structures. The large reaction free energies calculated indicate that the reactions are very exergonic. The

Scheme 3. Proposed Mechanism for the Formation of **2**−**5**

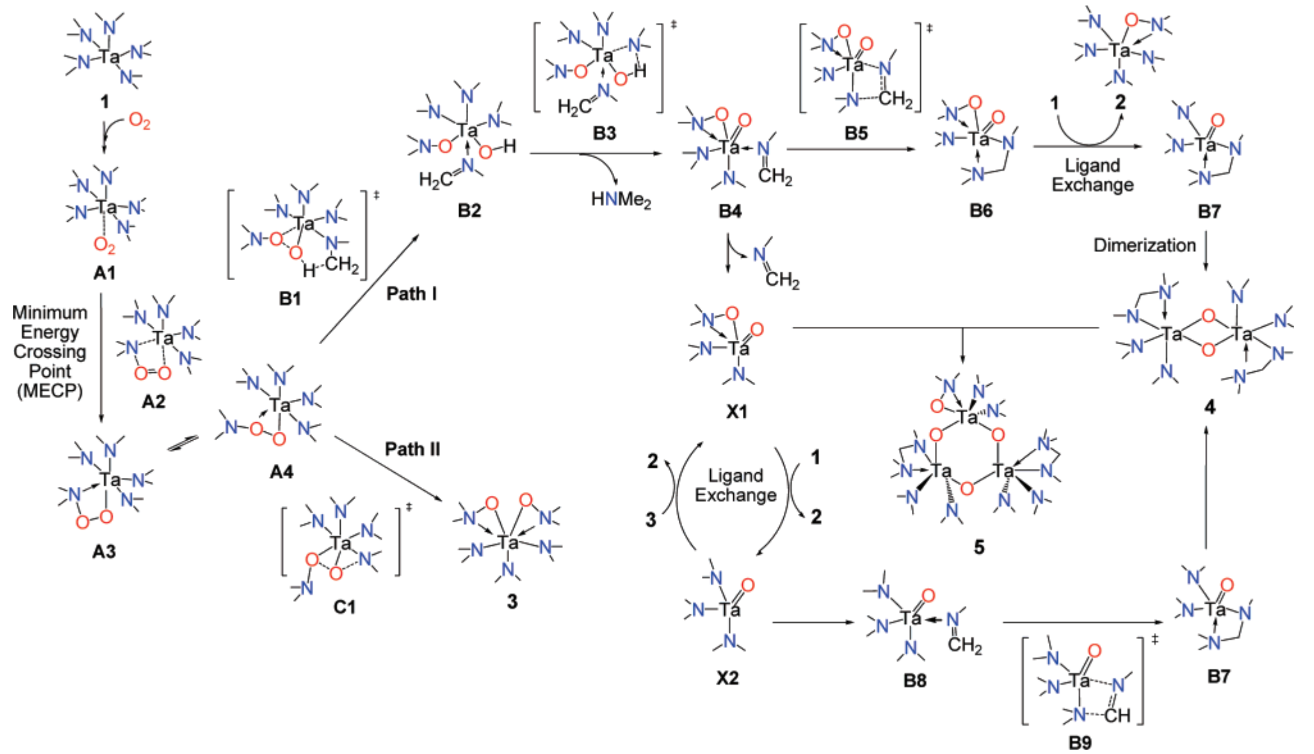

mechanisms are proposed here for the formation of **2**−**5** in the reaction of $Ta(NMe_2)_5$ (**1**) with O_2.

Proposed Reaction Mechanism. On the basis of the calculation results, we proposed the reaction mechanisms to account for the formation of **2**−**5** (Scheme 3). The reaction is initiated by the insertion of the triplet O_2 into one of the Ta−N bonds in $Ta(NMe_2)_5$ (**1**) through minimum energy crossing point (MECP)[20] **A2** to produce the tantalum peroxide **A3**. **A3** easily isomerizes to **A4**. Then the peroxide ligand of **A4** oxidizes one amide ligand by two competitive reaction pathways. The predominant one is Path II, in which the two-coordinate, Ta-bonded O of the peroxide ligand attacks the N of the nearby amide ligand to form **3** directly. The other pathway is Path I, in which the two-coordinate O abstracts a hydride from the nearby amide ligand followed by a proton transfer to eliminate an amine to give the Ta−oxo species **B4**. **B4** sequentially undergoes coupling reaction (**B4** → **B6** via **B5**), ligand exchange (**B6** + **1** → **B7** + **2**), and dimerization (2 **B7** → **4**) to form **4**. **2** can be obtained from the following three ligand-exchange reactions: **B6** + **1** → **B7** + **2**, **X1** + **1** → **X2** + **2**, and **X2** + **3** → **X1** + **2** (Scheme 3). Via imine insertion, the transient species **X2** also affords **B7**, which can dimerize to form **4**. The complexation of **4** and **X1** leads to the formation of **5**. The detailed calculation results that lead to the proposed mechanism are described below.

Insertion of O_2 into a Ta−N Bond in $Ta(NMe_2)_5$ (1). In a previous study, we found that O_2 reacts with $Zr(NMe_2)_4$ via a dimeric pathway rather than a monomeric pathway.[10] Our calculations show that, different from the group 4 analogues $M(NMe_2)_4$ (M = Zr, Hf), $Ta(NMe_2)_5$ (**1**), containing one more amide ligand, cannot dimerize because of its crowded coordination sphere. An end-on O_2 complex (Chart 1[14]) could not be located. On the basis of these results, it is concluded that $Ta(NMe_2)_5$ (**1**) can only react with O_2 via a monomeric pathway.

Chart 1

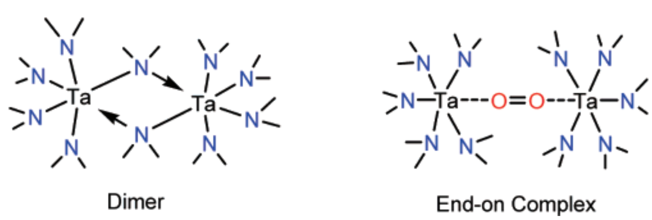

The van der Waals complex **A1** (Scheme 3 and Figure 4) formed between $Ta(NMe_2)_5$ (**1**) and the triplet O_2 has long Ta−O distances (ca. 4.4 Å). To reach the singlet energy surface, an intersystem conversion from triplet to singlet energy surface occurs at the MECP. The MECP, **A2**, was located with a program code developed by Harvey and co-workers.[20d,e] **A2** is not a stationary point on the potential energy surface, and its energy cannot be corrected with ZPE correction. The MECP (**A2**) is ca. 14.9 kcal/mol higher in electronic energy than **1** + triplet O_2, which is set to be the reference state. The entropy loss for the formation of **A2** is expected to be between those of **A1** and **A3**. Therefore, the relative free energy of **A2** with respect to the reference state is estimated to be ca. 25 kcal/mol. The result suggests that formation of **A3** is viable under the reaction conditions. Through this triplet−singlet crossover at the structure **A2**, the singlet Ta peroxide **A3** is formed with a reaction energy of −13.0 kcal/mol. In this process, the amide ligand is oxidized. After the O−O insertion into the Ta−N bond, the "leaving" amide forms a dative bond with the Ta center.

(19) The X-ray structural parameters of **1** are from its structure in Batsanov, A. S.; Churakov, A. V.; Howard, J. A. K.; Hughes, A. K.; Johnson, A. L.; Kingsley, A. J.; Neretin, I. S.; Wade, K. *J. Chem. Soc., Dalton Trans.* **1999**, 3867.

(20) (a) Schröder, D.; Shaik, S.; Schwarz, H. *Acc. Chem. Res.* **2000**, *33*, 139. (b) Poli, R.; Harvey, J. N. *Chem. Soc. Rev.* **2003**, *32*, 1. (c) Harvey, J. N. *Phys. Chem. Chem. Phys.* **2007**, *9*, 331. (d) Harvey, J. N.; Aschi, M.; Schwarz, H.; Koch, W. *Theor. Chem. Acc.* **1998**, *99*, 95. (e) Harvey, J. N.; Aschi, M. *Phys. Chem. Chem. Phys.* **1999**, *1*, 5555.

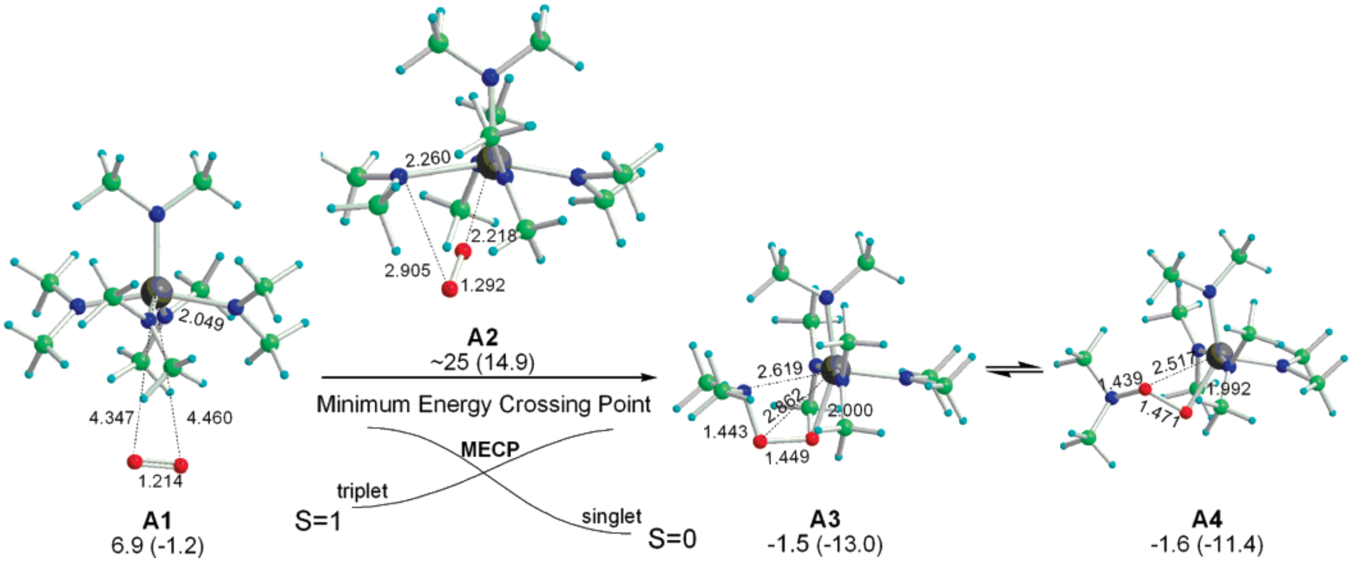

Figure 4. Calculated relative free energies and optimized structures of **A1**, **A2**, **A3**, and **A4**. The relative free energies and electronic energies (in parentheses) are given in kcal/mol. The bond lengths are in Å.

The peroxide ligand −O−O−NMe_2 formed from the O_2 insertion step can also form a dative bond with the Ta center from the other donor, O atom. By rotating the O−O bond, **A3** rearranges to **A4**, which has a similar stability with **A3**. Coordination of both the two oxygen atoms of the peroxide ligand to the Ta center elongates the O−O bond, giving a situation wherein the O−O bond is easier to be cleaved in this isomer.

Possible Pathways for Hydrogen Migration and Amine Elimination. Reaction of O_2 with **1** leads to the formation of **2**−**5** with the η^2-N(Me)CH_2NMe_2 ligand in **4** and **5**. To generate this interesting ligand, it is convenient to think of a pathway that involves a β-H migration from a NMe_2 ligand to one of the other ligands or to the metal center, leading to the formation of a MeN═CH_2 ligand, followed by a nucleophilic attack of another NMe_2 ligand on the carbon center of the newly formed MeN═CH_2 ligand. β-H abstraction by another amide ligand is well-known and is attributed, e.g., to the formation of $Ta(NEt_2)_3$-(EtN═CHMe)[21a] and in the D incorporation from $DN(CH_3)_2$, in presence of $M(NMe_2)_n$, into the methyl group, yielding (CH_3)-(CH_2D)NH.[21b] In the current case, several possible precursor complexes, **1**, **A3**, **A4**, **2**, and **3**, are able to undergo the β-H migration followed by the nucleophilic attack. All of these possible hydrogen migration pathways were examined thoroughly.

Four types of hydrogen migration transition structures based on the five precursor complexes mentioned above are shown in Figure 5. Transition structure **I**, in a β-H abstraction process, is based on the precursor complex **1**. Since **1** adopts a square pyramidal geometry, the amides are not equivalent. Different

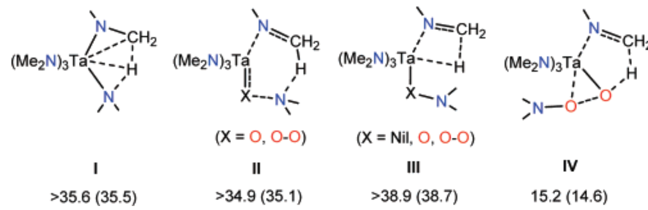

Figure 5. Four types of possible hydrogen migration transition states. The activation free energies and electronic energies (in parentheses), which are relative to their corresponding precursor complexes, are given in kcal/mol.

isomeric transition structures were calculated. The lowest barrier for this type of hydrogen migration is ca. 35 kcal/mol. The barriers are similar to those we obtained previously for cases with a hydrogen migration from a methyl group.[22] In the five-membered-ring transition structures (**I**), the metal center interacts with all of the other four members. The hydrogen migration resembles a σ-bond metathesis between a C−H bond and a Ta−N bond.

The situation is different in transition structure **II**. The hydrogen migration involves a hydride rather than a proton, leading to the breaking of both the C−H and X−N bonds. The hydride migration liberates $HNMe_2$ and gives a Ta−oxo if X = O or a Ta−peroxide if X = O−O. The transition structure **II**, in which the NMe_2 group in the six-membered ring does not have a bonding interaction with the metal center, are also high in energy. The results are expected because a NMe_2 group without metal coordination is not a good hydride acceptor.

Transition structure **III** corresponds to a stepwise process, β-H elimination followed by hydride migration. Formation of the Ta−H intermediates is a very endothermic process, leading to even higher barriers (>39 kcal/mol).

The most favorable hydrogen migration is the β-H migration process involving the transition structure **IV**, which corresponds to the **A4** to **B2** conversion shown in Scheme 3 and Figure 6. During this process, the peroxide ligand oxidizes the amide to imine through the abstraction of a hydride, while the peroxide

(21) (a) Takahashi, Y.; Onoyama, N.; Ishikawa, Y.; Motojima, S.; Sugiyama, K. *Chem. Lett.* **1978**, 525. (b) Nugent, W. A.; Ovenall, D. W.; Holmes, S. J. *Organometallics* **1983**, *2*, 161. For other examples of β-H abstraction reactions to give imine ligands, see: (c) Berno, P.; Gambarotta, S. *Organometallics* **1995**, *14*, 2159. (d) Scoles, L.; Ruppa, K. B. P.; Gambarotta, S. *J. Am. Chem. Soc.* **1996**, *118*, 2529. (e) Tsai, Y.-C.; Johnson, M. J. A.; Mindiola, D. J.; Cummins, C. C.; Klooster, W. T.; Koetzle, T. F. *J. Am. Chem. Soc.* **1999**, *121*, 10426. (f) Rothwell, I. P. *Polyhedron* **1985**, *4*, 177. (g) Ahmed, K. J.; Chisholm, M. H.; Folting, K.; Huffman, J. C. *J. Am. Chem. Soc.* **1986**, *108*, 989. (h) Airoldi, C.; Bradley, D. C.; Vuru, G. *Transition Met. Chem.* **1979**, *4*, 64. (i) Mayer, J. M.; Curtis, C. J.; Bercaw, J. E. *J. Am. Chem. Soc.* **1983**, *105*, 2651. (j) Bürger, H.; Neese, H.-J. *J. Organomet. Chem.* **1970**, *21*, 381. (k) de Castro, I.; Galakhov, M. V.; Gómez, M.; Gómez-Sal, P.; Royo, P. *Organometallics* **1996**, *15*, 1362.

(22) (a) Wu, Y.-D.; Chan, K. W. K.; Xue, Z.-L. *J. Am. Chem. Soc.* **1995**, *117*, 9259. (b) Wu, Y.-D.; Peng, Z.-H.; Xue, Z.-L. *J. Am. Chem. Soc.* **1996**, *118*, 9772. (c) Yu, X.; Bi, S.; Guzei, I. A.; Lin, Z.; Xue, Z.-L. *Inorg. Chem.* **2004**, *43*, 7111.

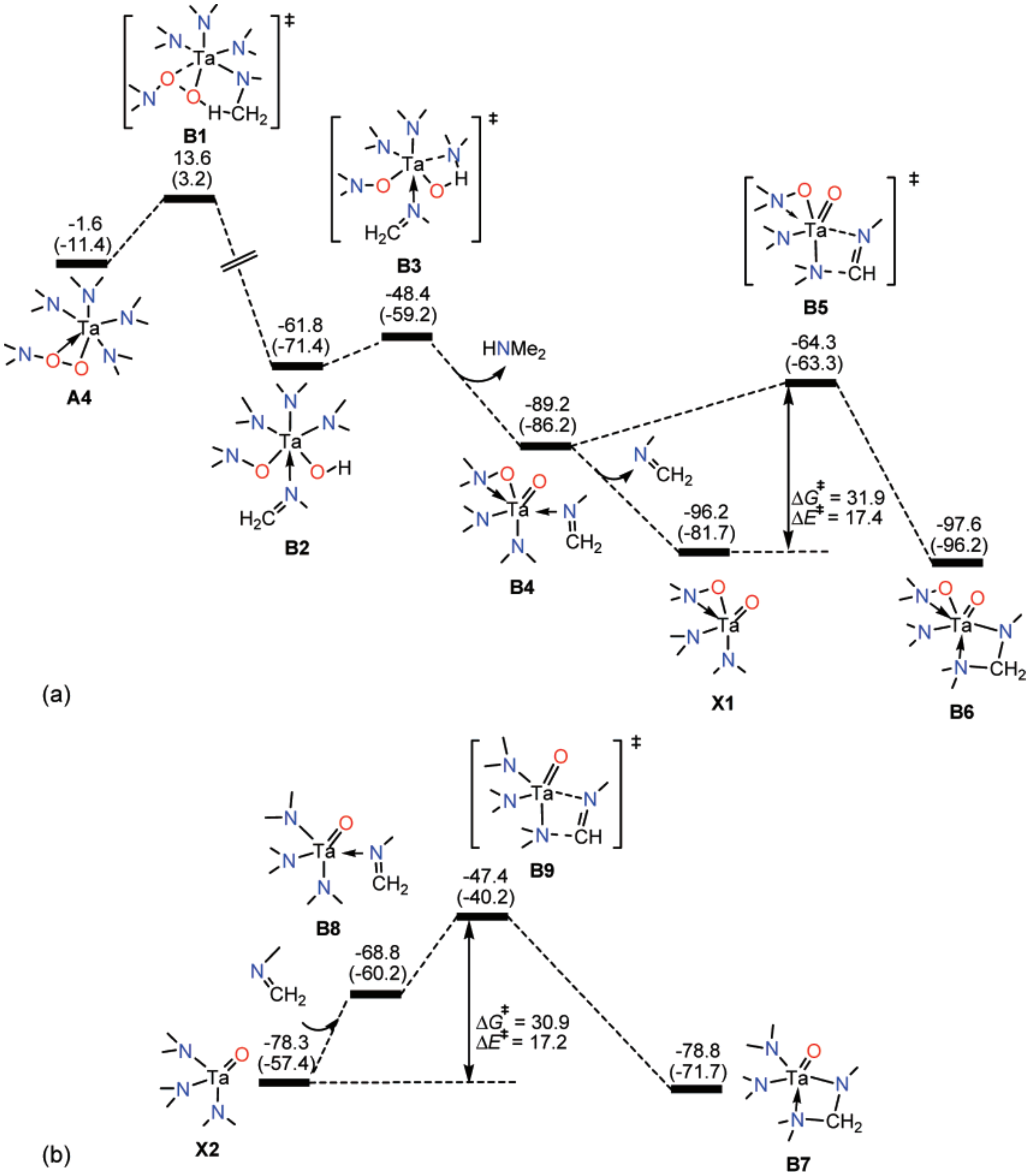

Figure 6. Calculated energy profile for the most favorable hydrogen migration reaction. The relative free energies and electronic energies (in parentheses) are given in kcal/mol.

itself is reduced to a hydroxide ligand and an aminoxide ligand. The proton of the hydroxide ligand in **B2** is considered to be quite acidic and can be easily transferred to a neighboring amide to complete the $HNMe_2$ elimination, resulting in the formation of the stable intermediate, Ta−oxo complex **B4** (Scheme 3 and Figure 6). The −OH proton transfer leading to the elimination of $HNMe_2$ from $Ta(NMe_2)_5$ (**1**) was reported in other complexes as well.[23] Both the hydride migration (**A4** → **B2**) and the proton transfer (**B2** → **B4**) have low activation energies and are very exothermic, suggesting that the peroxide ligand plays an important role. The importance of the peroxide ligand may explain the other oxidation reactions between O_2 and metal amides that involve amine eliminations.

(23) (a) Schweiger, S. W.; Tillison, D. L.; Thorn, M. G.; Fanwick, P. E.; Rothwell, I. P. *J. Chem. Soc., Dalton Trans.* **2001**, 2401. (b) Fei, Z.; Busse, S.; Edelmann, F. T. *J. Chem. Soc., Dalton Trans.* **2002**, 2587.

Formation of the η^2-N(Me)CH_2NMe_2 Ligand in 4. The dissociation of the imine ligand from the Ta complex **B4** affords a five-coordinate Ta complex **X1**. **X1** is a coordinatively unsaturated Ta−oxo complex and tends to form O-bridging complexes with other Ta complexes, making it act as a catalyst in ligand-exchange reactions. By exchanging the $-ONMe_2$ ligand with **1**, **X1** transforms to another Ta−oxo complex **X2**. The details of the ligand exchange will be discussed later. The relatively spacious environment of **X1** and **X2** provides a possibility for the coordination of imine ligand (**B4** and **B8**) and the following imine ligand insertion. In transition state **B5** or **B9**, the imine inserts into one of the Ta−N bonds to give the intermediate Ta−oxo complex, **B6** or **B7**, containing the interesting η^2-N(Me)CH_2NMe_2 ligand. These insertion processes are exothermic with activation free energies of ca. 31 kcal/mol (Figure 6). The gas-phase calculation tends to overestimate the

Scheme 4

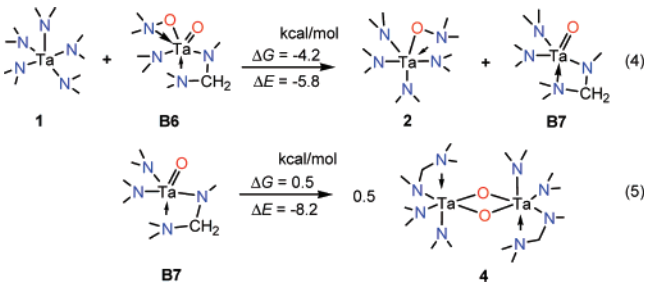

entropy loss of bimolecular reactions, and consequently to overestimate the activation free energies. Therefore, the barriers of the insertion step are expected to be lower than 31 kcal/mol and feasible. Similar to **X1**, the intermediate oxo complex **B6** is flexible to create a coordination-unsaturated environment around the metal center, allowing a ligand-exchange reaction to occur. The ligand exchange, which will be discussed later, occurs between **B6** and **1** to form **B7** and **2** (Scheme 4). **B7** is in fact a monomer of the dimer **4**. The dimerization energy of **B7** is ca. 8.2 kcal/mol, enough to compensate the entropy loss of the dimerization process. The calculated dimerization free energy is close to zero, suggesting that **B7** and **4** are in equilibrium.

Formation of 3. In Path I, the reactive peroxide bond of **A4** breaks, facilitating the O−H bond formation (**A4** → **B2**). In Path II, the peroxide bond cleavage also plays an important role in the formation of **3**. In the peroxide bond cleavage, the pathway from **A4** is much more favorable than that directly from **A3** (Figure 7). In the much more favorable pathway, the three-coordinate O facilitates the peroxide bond cleavage.[10]

Ligand Exchange and Formation of 2. Formation of **2** requires that the two O atoms of O_2 are separated into two molecules. Since complexation of O_2 with 2 equiv of **1** is unlikely to take place, the separation of the two O atoms into two molecules can be achieved with a ligand exchange between an O-containing Ta complex and an O-free Ta complex. A careful examination of all mononuclear complexes or intermediates we have discussed thus far indicates that a few oxo intermediates, which have a less crowded ligand environment, are suitable to undergo ligand-exchange reactions with the five-coordinated complex $Ta(NMe_2)_5$ (**1**). These oxo intermediates can rearrange themselves to four-coordinate species, providing a vacant coordination site for binding with **1**. Another reason to consider these oxo intermediates is that an early transition metal−oxo bond can easily transform itself to a bridging oxo that links two metal centers.[24] As discussed above, **2** can be generated from the ligand exchange between **1** and **B6**, an oxo intermediate. Equation 6 in Scheme 5 shows the energetics related to the ligand exchange. The complex **Com-B6−1** is formed with two bridging ligands; one is the oxo of **B6**, and the other is an amide of **1**. **Com-B6−1** can transform to **Com-B7−2** by switching the bridging ligand from the amide to the aminoxide. Then **Com-B7−2** decomposes into two new species **B7** and **2**, completing the ligand-exchange process. The fact that the ligand-exchange reaction is exothermic together with the stability of **Com-B6−1** and **Com-B7−2** suggests that the ligand exchange is feasible.

If the ligand-exchange reaction in eq 4 is the only reaction that produces **2**, then **2** is supposed to be two equiv of **4**. However, the experimental results of the yields of **2** and **4** are 26−27% and 9−10% (by NMR, 1 equiv of O_2), respectively, indicating that there may be other pathways for the formation of **2**. **X1** generated from the imine dissociation of **B4** (shown in Figure 6) is another Ta−oxo intermediate that is able to undergo ligand exchange with $Ta(NMe_2)_5$ (**1**). Since there is

Scheme 5. Calculated Relative Energies for Species Involved in the Ligand Exchange Reactions

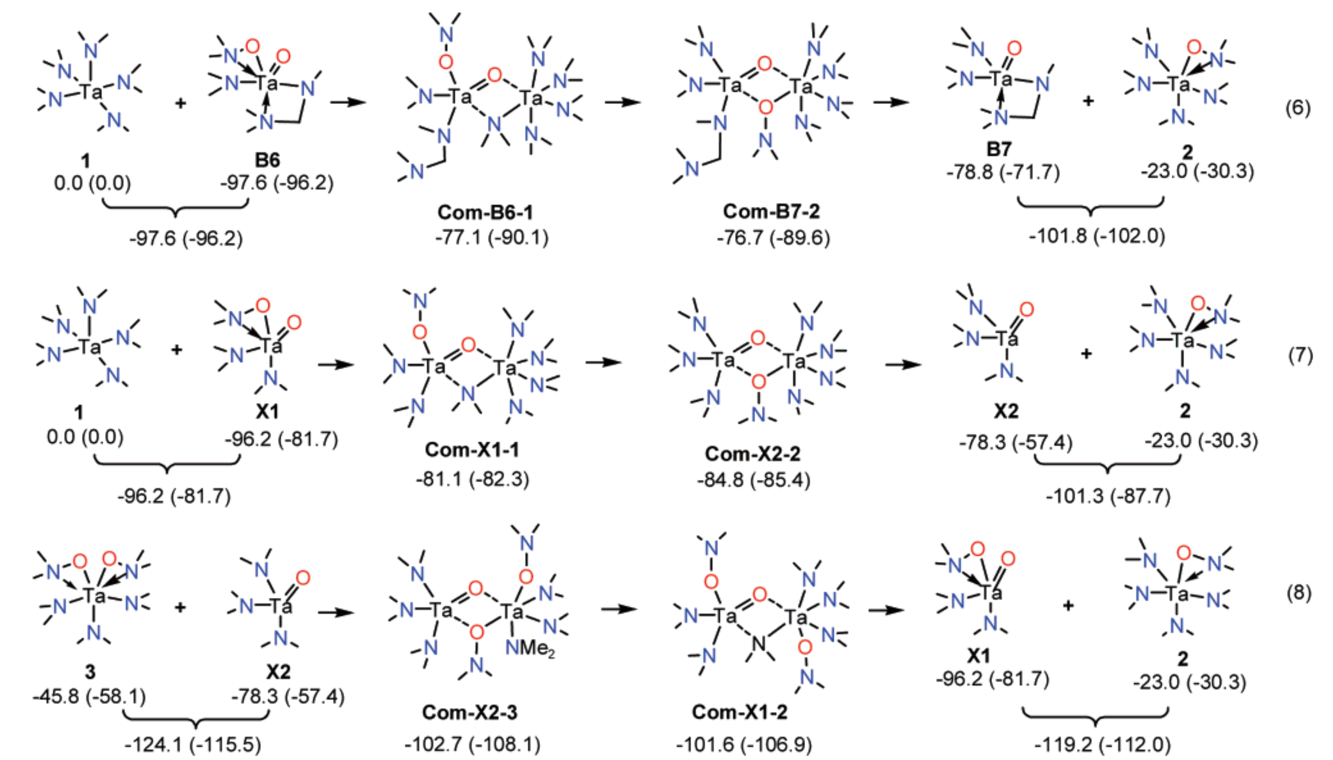

[a] Relative free energies and electronic energies (in parentheses) are given in kcal/mol.

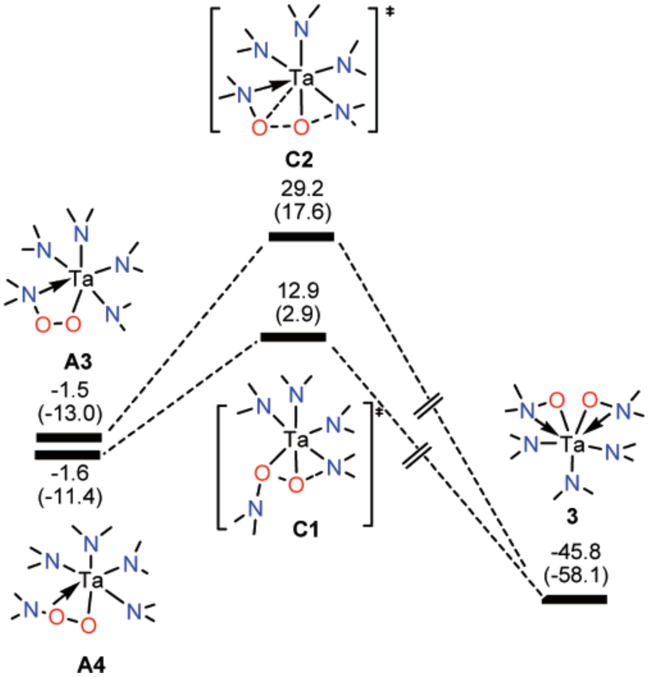

Figure 7. Calculated energy profile for the peroxide bond cleavage reaction. The relative free energies and electronic energies (in parentheses) are given in kcal/mol.

only a small amount of **X1** in the solution, instead of dimerization it can easily react with the relatively abundant **1**. Equation 7 in Scheme 5 shows that complexation of **X1** with **1** gives **Com-X1−1** and then **Com-X2−2**. The **X1−1** binding energies in these two complexes are greater than the **B6−1** binding energies in **Com-B6**−1 and **Com-B7−2**, suggesting a lower barrier for this ligand-exchange process. This ligand-exchange reaction gives **2** and **X2** with a reaction free energy of ca. −6.0 kcal/mol. **X2** is another Ta−oxo complex that has a less crowded ligand environment. The ligand exchange between **X2** and the relatively abundant species **3** can give **2** and **X1**. The two ligand-exchange reactions (**1** + **X1** → **2** + **X2** and **X2** + **3** → **2** + **X1**) form a thermodynamically favorable catalytic cycle, leading to the formation of **2**, as shown in eq 9 (see also Scheme 3).

$$\mathbf{1} + \mathbf{3} \xrightarrow{\mathbf{X1}\ \text{(cat.)}} \mathbf{2} + \mathbf{2} \qquad \begin{array}{l} \Delta G = -0.2\ \text{kcal/mol} \\ \Delta E = -2.7\ \text{kcal/mol} \end{array} \qquad (9)$$

Experimentally, the mixture of **3** and **1** gives **2** under a fairly harsh condition, 90 °C, suggesting that the direct ligand exchange[15] is difficult to take place. Therefore, a catalyst, such as the Ta−oxo intermediate **X1** or **X2**, is necessary for this process.

Formation of 5. Because of the high tendency to complex with other species, the Ta−oxo intermediates **X1** and **X2** were not detected. However, the existence of the transient speice **X1** was supported by the observation of **5**. **5** is composed of **4** and **X1** formally. The complexation of **4** and **X1** is found to be quite exothermic (eq 10).

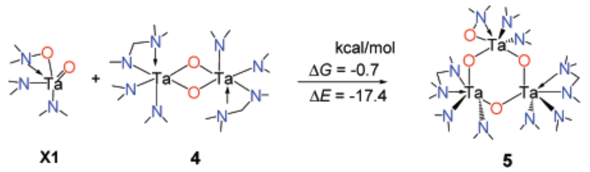

(10)

Conclusions

The formation of an unusual oxo−amino complex $(Me_2N)_4Ta_2[\eta^2\text{-}N(Me)CH_2NMe_2]_2(\mu\text{-}O)_2$ (**4**) and $(Me_2N)_6Ta_3[\eta^2\text{-}N(Me)CH_2NMe_2]_2(\eta^2\text{-}ONMe_2)(\mu\text{-}O)_3$ (**5**) containing novel chelating $-N(Me)CH_2NMe_2$ ligands, aminoxy complexes $(Me_2N)_4Ta(\eta^2\text{-}ONMe_2)$ (**2**) and $(Me_2N)_3Ta(\eta^2\text{-}ONMe_2)_2$ (**3**) implies three key steps in the reactions of $Ta(NMe_2)_5$ (**1**) with triplet O_2: (i) formation of a peroxide ligand from the oxygen insertion into Ta−N bonds; (ii) cleavage of O−O bond in the peroxide $O-O-NMe_2$ ligands to form two aminoxy ligands or one aminoxy as well as one Ta═O ligand; (iii) exchange between amino and aminoxy ligands. The ligands formed from these three steps are elementary steps in the formation of metal oxides from the reaction of d^0 metal amides with triplet O_2.

A detailed theoretical study indicates that the formation of **2**−**5** is initiated by O_2 insertion into monomeric $Ta(NMe_2)_5$ (**1**), through an intersystem conversion from triplet to singlet energy surface to form the active peroxide complex **A4**. This peroxide complex undergoes two competitive reactions: A majority of **A4** undergo peroxide bond cleavage via Path II to produce **3** which is the product with the highest yield (37% by NMR). A minority of **A4** proceed via Path I and ultimately gives **4** and **3** at the ratio of 1:2. A small amount of **2** is also obtained from the catalytic ligand exchange reaction between **3** and **1**. Although a study using a radical trap did not reveal the formation of trapped radicals, autoxidation involving radicals as an alternative pathway needs to be further explored in detail in the future.

Experimental Section

General Procedures. All manipulations were performed under a dry and oxygen-free nitrogen atmosphere with the use of glovebox or Schlenk techniques. All solvents were purified by distillation from potassium/benzophenone ketyl. Benzene-d_6 and toluene-d_8 were dried and stored over activated molecular sieves under nitrogen. $TaCl_5$ (Strem), $Me_2NOH{\cdot}HCl$ (Aldrich), liquid ammonia (Air Products & Chemicals, Inc.), O_2 (National Welders Supply Co.), dried by passing a P_2O_5 column, and $LiNMe_2$ (Aldrich) were used as received. $Ta(NMe_2)_5$ (**1**), $Ta(NMe_2)_4Cl$, $Ta(NMe_2)_3Cl_2$, and $LiONMe_2$ were made according to the references.[15,25−27] NMR spectra were recorded on a Bruker AMX-400 Fourier transform spectrometer. Elemental analyses were conducted by Complete Analysis Laboratories, Inc., Parsippany, NJ. *Caution: Several studies below were conducted in heated, sealed Young NMR tubes. New NMR tubes should be used, and the heating should be performed behind a protective shield.*

Preparation of $(Me_2N)_4Ta(\eta^2\text{-}ONMe_2)$ (2), $(Me_2N)_3Ta(\eta^2\text{-}ONMe_2)_2$ (3), $(Me_2N)_4Ta_2[\eta^2\text{-}N(Me)CH_2NMe_2]_2(\mu\text{-}O)_2$ (4), and $(Me_2N)_6Ta_3[\eta^2\text{-}N(Me)CH_2NMe_2]_2(\eta^2\text{-}ONMe_2)(\mu\text{-}O)_3$ (5). A solution of $Ta(NMe_2)_5$ (**1**, 1.969 g, 4.91 mmol) in toluene or benzene (30.0 mL) was frozen in liquid nitrogen, and the Schlenk flask was pumped for 10 min. The frozen solid was warmed gradually till it melted, and 0.5 equiv of O_2 (2.45 mmol) was then added. The yellow solution was stirred overnight

(24) (a) Abbenhuis, H. C. L.; Feiken, N.; Grove, D. M.; Jastrzebski, J. T. B. H.; Kooijman, H.; der Sluis, P. V.; Smeets, W. J. J.; Spek, A. L.; Van Koten, G. *J. Am. Chem. Soc.* **1992**, *114*, 9773. (b) Jernakoff, P.; de Bellefon, C. D.; Geoffroy, G. L.; Rheingold, A. L.; Geib, S. J. *Organometallics* **1987**, *6*, 1362. (c) Sánchez-Nieves, J.; Frutos, L. M.; Royo, P.; Castaño, O.; Herdtweck, E. *Organometallics* **2005**, *24*, 2004.

(25) Bradley, D. C.; Thomas, I. M. *Can. J. Chem.* **1962**, *40*, 1355.
(26) Chisholm, M. H.; Tan, L.-S.; Huffman, J. C. *J. Am. Chem. Soc.* **1982**, *104*, 4879.
(27) Mitzel, N. W.; Losehand, V.; Wu, A.; Cremer, D.; Rankin, D. W. H. *J. Am. Chem. Soc.* **2000**, *122*, 4471.

at room temperature. A small amount of white precipitation was observed. All volatiles were removed in vacuo to leave a yellow oil which was extracted with *n*-pentane. The filtrate was concentrated and recrystallized at −32 °C to first give colorless crystals of (Me$_2$N)$_4$Ta$_2$[η^2-N(Me)CH$_2$NMe$_2$]$_2$(μ-O)$_2$ (**4**, 0.128 g, 0.172 mmol, 7% yield based on O$_2$) in a few days. ^{1}H NMR of **4** (benzene-d_6, 400.18 MHz, 23 °C) δ 4.19 (s, 4H, 2C*H*$_2$), 3.51 (s, 24H, 4N*Me*$_2$), 3.22 (s, 6H, 2N*Me*-CH$_2$), 2.39 (s, 12H, 2CH$_2$−N*Me*$_2$). ^{13}C NMR (benzene-d_6, 100.63 MHz, 23 °C) δ 83.06 (2*C*H$_2$), 48.06 (2CH$_2$−N*Me*$_2$), 46.88 (4N*Me*$_2$), 38.66 (2N*Me*−CH$_2$). Anal. Calcd for C$_{16}$H$_{46}$N$_8$O$_2$Ta$_2$: C, 25.81; H, 6.23. Found: C, 25.64; H, 6.19.

After the crystals of **4** were collected, the supernatant solution was concentrated to afford a yellow oil which was sublimed at 55 °C under reduced pressure to give a solid of (Me$_2$N)$_4$Ta(η^2-ONMe$_2$) (**2**) (0.560 g, 1.342 mmol, 27% yield based on O$_2$) on a cold finger. This pale-yellow solid was dissolved in Et$_2$O, and the solution was cooled to −32 °C to give colorless crystals of (Me$_2$N)$_4$Ta(η^2-ONMe$_2$) (**2**). ^{1}H NMR of **2** (benzene-d_6, 400.18 MHz, 23 °C) δ 3.25 (s, 24H, 4N*Me*$_2$), 2.47 (s, 6H, ON*Me*$_2$). ^{13}C NMR (benzene-d_6, 100.63 MHz, 23 °C) δ 48.80 (s, 4N*Me*$_2$), 47.04 (s, ON*Me*$_2$). Anal. Calcd for C$_{10}$H$_{30}$N$_5$O$_2$Ta: C, 28.78; H, 7.25. Found: C, 28.49; H, 7.17.

After sublimation of **2**, the yellow residue was dissolved in a small amount of *n*-pentane again. A few days later, some colorless crystals of (Me$_2$N)$_3$Ta(η^2-ONMe$_2$)$_2$ (**3**) (0.130 g, 0.300 mmol, 12% yield based on O$_2$) came out at −32 °C. ^{1}H NMR of **3** (benzene-d_6, 400.18 MHz, 23 °C) δ 3.41 (s, 6H, N*Me*$_2$), 3.05 (s, 6H, 2N*Me*$_A$Me$_B$), 2.94 (s, 6H, 2NMe$_A$*Me*$_B$), 2.56 (s, 12H, 2ON*Me*$_2$). ^{13}C NMR (benzene-d_6, 100.63 MHz, 23 °C) δ 50.14 (s, 2ON*Me*$_2$), 48.98 (s, N*Me*$_2$), 47.05 (s, 2N*Me*$_A$-Me$_B$), 46.11 (s, 2NMe$_A$*Me*$_B$). Anal. Calcd for C$_{10}$H$_{30}$N$_5$O$_2$Ta: C, 27.72; H, 6.98. Found: C, 27.49; H, 6.75.

A few crystals of **5** were sometimes found along with those of **4** from the reaction Ta(NMe$_2$)$_5$ (**1**) with 0.5 equiv of O$_2$. However, ^{1}H NMR spectrum of the crystals showed only resonances of **4**. A higher yield of **5** was obtained from the reaction of 4 equiv of O$_2$ with **1**. ^{1}H NMR spectra of the mixture of crystals gave the resonances of **5** (and **4**). In this reaction, 4 equiv of O$_2$ was added to a solution of **1** (0.75 g, 1.87 mmol) by a procedure similar to that in the reaction of **1** with 0.5 equiv of O$_2$. Crystallization gave a mixture of crystals (67 mg) of **4** and **5** in a molar ratio of **4**:**5** = 26:1 (5.5 wt % **5**; 3.7 mg, 0.0033 mmol, 0.52% yield of **5** based on **1**) by ^{1}H NMR. Attempts to separate the two crystals were not successful, as they appeared similar. ^{1}H NMR of **5** (toluene-d_8, 400.18 MHz, 23 °C) δ 4.14−3.93 (m, 4H, C*H*$_A$*H*$_B$ and C*H*$_C$*H*$_D$), 3.71 (s, 6H, N*Me*$_2$), 3.64 (s, 6H, N*Me*$_2$), 3.60 (s, 6H, N*Me*$_2$), 3.39 (s, 6H, N*Me*$_2$), 3.32 (s, 6H, N*Me*$_2$), 3.31 (s, 6H, N*Me*$_2$), 3.17 (s, 3H, N*Me*-CH$_2$), 3.08 (s, 3H, N*Me*-CH$_2$), 2.31 (s, 6H, ON*Me*$_2$), 2.21 (s, 6H, CH$_2$−N*Me*$_2$), 2.12 (s, 6H, CH$_2$−N*Me*$_2$). ^{13}C NMR (toluene-d_8, 100.63 MHz, 23 °C) δ 82.84 (*C*H$_2$), 82.00 (*C*H$_2$), 48.25−47.19 (6N*Me*$_2$), 47.16 (ON*Me*$_2$), 46.37 (N*Me*$_2$-CH$_2$), 46.09 (N*Me*$_2$-CH$_2$), 39.04 (N*Me*-CH$_2$), 38.89 (N*Me*-CH$_2$). Anal. Calcd for a mixture of **4** and **5** [Molar ratio **4**: **5** = 26:1; C$_{22}$H$_{64}$N$_{11}$O$_4$Ta$_3$·1/2(toluene) or C$_{25.5}$H$_{68}$N$_{11}$O$_4$-Ta$_3$ (Calcd C, 26.97; H, 6.03) for **5**]: C, 25.85; H, 6.22. Found: C, 25.85; H, 6.16.

Reaction of excess O$_2$ with Ta(NMe$_2$)$_5$ (**1**) was also studied. To a solution of **1** (10.3 mg, 0.026 mmol) in toluene-d_8 (0.5 mL) in a Young NMR tube was added 4 equiv of O$_2$ (0.103 mmol) at −65 °C. Si(SiMe$_3$)$_4$ (1.0 mg) was used as the NMR internal standard. The NMR tube was inserted into a spectrometer precooled at −65 °C, and the reaction was monitored by ^{1}H NMR. Over a period of 1.5 h, the temperature was gradually raised from −65 to −25 °C. ^{1}H NMR spectra of the reaction mixture gave the following yields (based on the limiting reagent **1**): 42% for **2**, 2.6% for **3**, 9.0% for dimeric **4**, and 4.5% for trinuclear **5**.

Reaction of Ta(NMe$_2$)$_5$ (1) with 0.5 equiv of O$_2$ at −50 °C. A Young NMR tube was loaded with Ta(NMe$_2$)$_5$ (**1**, 66.2 mg, 0.164 mmol) in toluene-d_8 (0.5 mL). After the solution was chilled by liquid nitrogen and pumped for 10 min, it was placed in a −50 °C bath in a dry ice/ethanol. O$_2$ (1 atm, 0.5 equiv, 0.082 mmol) was added to the NMR tube, and the NMR tube was then placed in a precooled 400 MHz NMR spectrometer at −50 °C. (Me$_2$N)$_4$Ta(η^2-ONMe$_2$) (**2**) appeared first in the ^{1}H NMR spectrum in ca. 23 min after O$_2$ was added. (Me$_2$N)$_3$Ta(η^2-ONMe$_2$)$_2$ (**3**) and (Me$_2$N)$_4$Ta$_2$[η^2-N(Me)CH$_2$-NMe$_2$]$_2$(μ-O)$_2$ (**4**) appeared later in 40 min.

Reaction of Ta(NMe$_2$)$_5$ (1) with 0.5 equiv of O$_2$ at Different Pressures. Young NMR tubes were connected to glass tubings to give the required volumes. Three samples containing 43.5−77.2 mg of **1** in toluene-d_8 (0.5 mL) were prepared. O$_2$ (0.5 equiv) at 240 (Sample A), 500 (Sample B), and 760 mmHg (Sample C), respectively, was added at room temperature. The reaction was monitored by ^{1}H NMR.

Reaction of Ta(NMe$_2$)$_5$ (1) with O$_2$ in the Presence of TEMPO as a Radical Trap. TEMPO (57.2 mg, 0.36 mmol) and 4, 4′-dimethoxybiphenyl (4.2 mg, 0.019 mmol) as the internal standard (IS) were dissolved in benzene-d_6 (0.5 mL) in a Young NMR tube. After the ^{1}H NMR spectrum was taken, Ta(NMe$_2$)$_5$ (**1**, 36.2 mg, 0.090 mmol) was added. After 20 min, the ^{1}H NMR spectrum of the mixture was taken. Subsequently O$_2$ (0.090 mmol, 1.0 atm, 2.2 mL) was added to the mixture, and the NMR tube was shaken. After 60 min, the ^{1}H NMR spectrum was taken.

Preparation of 2 from Ta(NMe$_2$)$_4$Cl and LiONMe$_2$. LiONMe$_2$ (0.134 g, 2.00 mmol) in toluene (20.0 mL) was added dropwise with stirring to 1 equiv of Ta(NMe$_2$)$_4$Cl (0.784 g, 2.00 mmol) in toluene (20.0 mL) at room temperature. The solution was warmed up to 50 °C and continued to stir at this temperature for 20 h. The solvent was stripped off to give yellow solids, which were extracted with *n*-pentane. The yellow filtrate was concentrated and cooled to −32 °C to give the pale-yellow solid Ta(NMe$_2$)$_4$(η^2-ONMe$_2$) (**2**, 0.797 g, 95.5% yield).

Preparation of 3 from Ta(NMe$_2$)$_3$Cl$_2$ and LiONMe$_2$. LiONMe$_2$ (0.268 g, 4.00 mmol) in toluene (20.0 mL) was added dropwise with stirring to Ta(NMe$_2$)$_3$Cl$_2$ (0.768 g, 2.00 mmol) in toluene (20.0 mL) at room temperature. The solution was warmed to 50 °C and stirred at this temperature for 20 h. The volatiles removed to give yellow solids, which were extracted with hexanes. The pale-yellow filtrate was cooled to −32 °C to give a white solid of Ta(NMe$_2$)$_3$(η^2-ONMe$_2$)$_2$ (**3**, 0.747 g, 86.2% yield).

Preparation of 3 from the Reaction of (Me$_2$N)$_4$Ta(η^2-ONMe$_2$) (2) with O$_2$. (Me$_2$N)$_4$Ta(η^2-ONMe$_2$) (**2**, 24.6 mg, 0.0590 mmol) and 4,4′-bimethyldiphenyl (2.0 mg, 0.011 mmol) as internal standard were placed into a Young NMR tube with benzene-d_6 (ca. 0.5 mL) in a drybox. The solution was frozen by liquid nitrogen and pumped. The frozen solution was then warmed to liquid, and 1 equiv of O$_2$ was added. The NMR tube was shaken for 30 min at 23 °C and then placed at room temperature for 99 h. ^{1}H NMR spectrum of the solution showed **2** had converted **3** (10.9 mg, 0.0252 mmol, yield 42.8% based on **2**).

Ligand Exchange between Ta(NMe$_2$)$_5$ (1) and (Me$_2$N)$_3$Ta(η^2-ONMe$_2$)$_2$ (3). A Young NMR tube was added **1** (5.9 mg, 0.015 mmol), **2** (7.3 mg, 0.017 mmol), and bibenzyl (3.0 mg, 0.016 mmol, internal standard) in benzene-d_6 (0.5 mL). The mixture was heated at 50 °C for 4 days. Afterward its ^{1}H NMR spectrum revealed no significant changes in the concentrations of the complexes and formation of **2**. The mixture was then heated at 90 °C for additional 3 days in the sealed NMR tube. ^{1}H NMR spectrum of the solution revealed the presence of a significant amount of (Me$_2$N)$_4$Ta(η^2-ONMe$_2$) (**2**, 0.008 mmol).

Heating a Mixture of Ta(NMe$_2$)$_5$ (1) and LiONMe$_2$. To a Young NMR tube was added **1** (5.2 mg, 0.013 mmol), LiONMe$_2$ (1.2 mg, 0.018 mmol), and bibenzyl (3.4 mg, 0.019 mmol, internal standard) in benzene-d_6 (0.5 mL). The mixture was heated at 50 °C for 6 days, and no ligand exchange was observed between Ta(NMe$_2$)$_5$ (**1**) and LiONMe$_2$.

Ligand Exchange between Ta(NMe$_2$)$_5$ (1), (Me$_2$N)$_3$Ta(η^2-ONMe$_2$)$_2$ (3), and LiNMe$_2$. To a Young NMR tube was added **1** (6.8 mg, 0.017 mmol), **3** (7.8 mg, 0.018 mmol), LiNMe$_2$ (1 mg, 0.020 mmol), and bibenzyl (3.4 mg, 0.019 mmol, internal NMR standard) in benzene-d_6 (0.5 mL). After the mixture was heated at 50 °C for 21 h, $(Me_2N)_4Ta(\eta^2\text{-}ONMe_2)$ (**2**) was observed in ^{1}H NMR spectra. The concentrations of $Ta(NMe_2)_5$ (**1**) and $(Me_2N)_3Ta(\eta^2\text{-}ONMe_2)_2$ (**3**) had increased and decreased, respectively. After heating the solution at 50 °C for another 6 days, ^{1}H NMR revealed that the concentrations of $(Me_2N)_4Ta(\eta^2\text{-}ONMe_2)$ (**2**) (0.0066 mmol) and **1** (0.021 mmol) had increased, and the concentration of $(Me_2N)_3Ta(\eta^2\text{-}ONMe_2)_2$ (**3**) (0.0080 mmol) had decreased. The NMR tube was then placed at room temperature, and no further change was observed.

Variable-Temperature NMR Studies of $(Me_2N)_3Ta(\eta^2\text{-}ONMe_2)_2$ (3). ^{1}H NMR spectra of a solution of **3** (15 mg) in benzene-d_6 (0.5 mL) in a Young NMR tube were taken at 296, 313, 333, and 343 K, respectively. These spectra are shown in Figure S4a−d.

Determination of X-ray Crystal Structures of 2−4. The data for the X-ray crystal structures of **4** were collected on a Bruker-AXS APEX diffractometer with Kryoflex low-temperature device, and the data of **2** and **3** were collected on a Smart 1000 X-ray diffractometer equipped with a CCD area detector fitted with an upgraded Nicolet LT-2 low-temperature device. The data were obtained using a graphite-monochromated Mo source ($K\alpha$ radiation, 0.71073 Å). Suitable crystals were coated with paratone oil (Exxon) and mounted on loops under a stream of nitrogen at the data collection temperature. The structures were solved by direct methods.

The systematic absences in the diffraction data were consistent with space groups $Pca2_1$ and $Pbcm$ for **2**, uniquely, $P2_1/n$ for **3**, and $C2$, Cm, and $C2/m$ for **4**. Only the noncentrosymmetric space group option in **4** yielded chemically reasonable and computationally stable results of refinement. Two symmetry unique but chemically similar molecules of **4** were located in the asymmetric unit. An inspection of the packing diagram does not show evidence of overlooked symmetry. The Flack parameter refined to nil, indicating the true hand of the data had been determined.

After thorough exploration of structural solutions in the space group options for **4**, only the solution in $C2/m$ yielded chemically reasonable and computationally stable results. The molecule in **4** was located at a two-fold axis and a mirror plane. Each Ta atom has two bridging O atoms, two terminal NMe_2 groups, and a chelating η^2-N(Me)CH_2NMe_2 ligand. One NMe_2 group is disordered by the mirror plane with part of the chelating η^2-N(Me)CH_2NMe_2 ligand.

Non-hydrogen atoms were anisotropically refined. All hydrogen atoms were treated as idealized contributions. Empirical absorption correction was performed with SADABS.[28a] In addition, the global refinements for the unit cells and data reductions of the two structures were performed using the Saint program (version 6.02). All calculations were performed using SHELXTL (version 5.1) proprietary software package.[28b]

Determination of X-ray Crystal Structure of 5. A colorless crystal with approximate dimensions $0.38 \times 0.34 \times 0.31$ mm^3 was selected under oil under ambient conditions and attached to the tip of a nylon loop. The crystal was mounted in a stream of cold nitrogen at 100(2) K and centered in the X-ray beam by using a video camera. The crystal evaluation and data collection were performed on a Bruker CCD-1000 diffractometer with Mo $K\alpha$ ($\lambda = 0.71073$ Å) radiation and the diffractometer to crystal distance of 4.9 cm.

The initial cell constants were obtained from three series of ω scans at different starting angles. Each series consisted of 20 frames collected at intervals of 0.3° in a 6° range about ω with the exposure time of 10 s per frame. A total of 64 reflections were obtained. The reflections were successfully indexed by an automated indexing routine built in the SMART program. The final cell constants were calculated from a set of 20191 strong reflections from the actual data collection.

The data were collected by using the full sphere data collection routine to survey the reciprocal space to the extent of a full sphere to a resolution of 0.72 Å. A total of 36051 data were harvested by collecting four sets of frames with 0.36° scans in ω and one set with 0.45° scans in φ with an exposure time 20 s per frame. These highly redundant datasets were corrected for Lorentz and polarization effects. The absorption correction was based on fitting a function to the empirical transmission surface as sampled by multiple equivalent measurements.[29]

The systematic absences in the diffraction data were consistent for the space groups $P\bar{1}$ and $P1$. The E-statistics strongly suggested the centrosymmetric space group $P\bar{1}$ that yielded chemically reasonable and computationally stable results of refinement.[29]

A successful solution by the direct methods provided most non-hydrogen atoms from the E-map. The remaining non-hydrogen atoms were located in an alternating series of least-squares cycles and difference Fourier maps. All non-hydrogen atoms were refined with anisotropic displacement coefficients. All hydrogen atoms were included in the structure factor calculation at idealized positions and were allowed to ride on the neighboring atoms with relative isotropic displacement coefficients.

There was one solvate molecule of toluene present in the asymmetric unit. A significant amount of time was invested in refining this molecule which was disordered over a crystallographic inversion center. Bond length restraints were applied to model the molecules, but the resulting isotropic displacement coefficients suggested the molecules were mobile. In addition, the refinement was computationally unstable. Option SQUEEZE of program PLATON[30] was used to correct the diffraction data for diffuse scattering effects and to identify the solvate molecule. PLATON calculated the upper limit of volume that can be occupied by the solvent to be 237 Å^3, or 12% of the unit cell volume. The program calculated 55 electrons in the unit cell for the diffuse species. This approximately corresponds to one molecule of toluene molecule in the asymmetric unit (50 electrons), or one-half molecule of solvent per trinuclear organometallic complex. Note that all derived results in the tables are based on the known contents. No data are given for the diffusely scattering species.

The final least-squares refinement of 381 parameters against 10805 data resulted in residuals R (based on F^2 for $I \geq 2\sigma$) and wR (based on F^2 for all data) of 0.0201 and 0.0505, respectively.

Computational Details. All calculations were performed using the Gaussian 03 package[31] with density functional theory (DFT) at the B3LYP level. Geometries were optimized with the following basis set: LanL2DZ with f polarization functions for Ta[32] and 6-31G* for the rest of elements. Vibration frequency calculations were performed on all the optimized structures with the same method to provide free energies at 298.15 K. The optimized minima and the transition structures have been confirmed by harmonic vibration frequency calculations. The calculated relative electronic energies shown in the text have been corrected with zero-point energies (ZPE). The minimum energy crossing point (MECP) was located with the code from Harvey.[20]

Acknowledgment is made to the National Science Foundation (CHE-0516928 to Z.X.), Research Grant Council of Hong Kong (HKUST6083/02M to Y.D.W. and HKUST 602304 to Z.L.), Camille Dreyfus Teacher-Scholar program (Z.X.), and the Royal Society (United Kingdom) Kan Tong Po Visiting Professorship for financial support of this work. We thank

(28) (a) Sheldrick, G. M. *SADABS*, A Program for Empirical Absorption Correction of Area Detector Data; University of Göttingen: Göttingen, Germany, 2000. (b) Sheldrick, G. M. *SHELXL-97*, A Program for the Refinement of Crystal Structures; University of Göttingen: Göttingen, Germany, 1997.

(29) SADABS V.2.05, SAINT V.6.22, SHELXTL V.6.10, and SMART 5.622 Software Reference Manuals: Bruker-AXS: Madison, Wisconsin, U.S.A., 2000−2003.

(30) Spek, A. L. *Acta Crystallogr.* **1990**, *A46*, C34.

(31) Frisch, M. J.; et al. *Gaussian 03*, Revision B.03; Gaussian, Inc.: Pittsburgh, PA, 2003. A complete author list is given in the Supporting Information.

(32) Ehlers, A. W.; Böhme, M.; Dapprich, S.; Gobbi, A.; Höllwarth, A.; Jonas, V.; Köhler, K. F.; Stegmann, R.; Veldkamp, A.; Frenking, G. *Chem. Phys. Lett.* **1993**, *208*, 111.

Professor Jeremy Harvey for sharing his program code to locate MECP, Prof. Liguo Song for the MS measurements, and Dr. Ruitao Wang for help.

Supporting Information Available: Experimental Section for MS analyses, 2D HMQC NMR spectra of **3** and **4**, variable-temperature and EXSY NMR spectra of **3**, ^{1}H NMR monitoring of the reactions between **1** and O_2 in the presence of TEMPO, crystallographic data of **2**−**5**, the optimized structures with total energies of the species in the proposed pathways, and complete ref 31. This material is available free of charge via the Internet at http://pubs.acs.org.

JA075076A